for Scientific Research from the Japanese Ministry of Health, Labour, and Welfare (MHLW).

Appendix A. Supplementary data

Supplementary data to this article can be found online at doi:10.1016/j.jconrel.2012.01.038.

References

[1] R. Duncan, The dawning era of polymer therapeutics, Nat. Rev. Drug Discov. 2 (2003) 347–360.
[2] M.E. Davis, Z. Chen, D. Shin, Nanoparticle therapeutics: an emerging treatment modality for cancer, Nat. Rev. Drug Discov. 7 (2008) 771–782.
[3] K. Kataoka, A. Harada, Y. Nagasaki, Block copolymer micelles for drug delivery: design, characterization and biological significance, Adv. Drug Deliv. Rev. 47 (2001) 113–131.
[4] N. Nishiyama, K. Kataoka, Current state, achievements, and future prospects of polymeric micelles as nanocarriers for drug and gene delivery, Pharmacol. Ther. 112 (2006) 630–648.
[5] H. Cabral, N. Nishiyama, K. Kataoka, Supramolecular nanodevices: from design validation to theranostic nanomedicine, Acc. Chem. Res. 44 (2011) 999–1008.
[6] Y. Matsumura, H. Maeda, A new concept for macromolecular therapeutics in cancer chemotherapy: mechanism of tumoritropic accumulation of proteins and the antitumor agent Smancs, Cancer Res. 46 (1986) 6387–6392.
[7] J.J. Gottlieb, K. Washenik, A. Chachoua, A. Friedman-Kien, Treatment of classic Kaposi's sarcoma with liposomal encapsulated doxorubicin, Lancet 350 (1997) 1363–1364.
[8] W.J. Gradishar, S. Tjulandin, N. Davidson, H. Shaw, N. Desai, P. Bhar, M. Hawkins, J. O'Shaughnessy, Phase III trial of nanoparticle albumin-bound paclitaxel compared with polyethylated castor oil-based paclitaxel in women with breast cancer, J. Clin. Oncol. 23 (2005) 7794–7803.
[9] M.R. Kano, Y. Bae, C. Iwata, Y. Morishita, M. Yashiro, M. Oka, T. Fujii, A. Komuro, K. Kiyono, M. Kaminishi, K. Hirakawa, Y. Ouchi, N. Nishiyama, K. Kataoka, K. Miyazono, Improvement of cancer-targeting therapy, using nanocarriers for intractable solid tumors by inhibition of TGF-β signaling, Proc. Natl. Acad. Sci. U. S. A. 104 (2007) 3460–3465.
[10] M.R. Kano, Y. Komuta, C. Iwata, M. Oka, Y.T. Shirai, Y. Morishita, Y. Ouchi, K. Kataoka, K. Miyanozo, Comparison of the effects of the kinase inhibitors imatinib, sorafenib, and transforming growth factor-β receptor inhibitor on extravasation of nanoparticles from neovasculature, Cancer Sci. 100 (2009) 173–180.
[11] K.D. Crew, A.I. Neugut, Epidemiology of gastric cancer, World J. Gastroenterol. 12 (2006) 354–362.
[12] E. Otsuji, Y. Kuriu, K. Okamoto, T. Ochiai, D. Ichikawa, A. Hagiwara, H. Yamagishi, Outcome of surgical treatment for patients with scirrhous carcinoma of the stomach, Am. J. Surg. 188 (2004) 327–332.
[13] Japanese Gastric, Cancer A Japanese classification of gastric carcinoma—2nd English Edition, Gastric Cancer 1 (1998) 10–24.
[14] Y. Hippo, M. Yashiro, M. Ishii, H. Taniguchi, S. Tsutumi, K. Hirakawa, T. Kosama, H. Aburatani, Differential gene expression profiles of scirrhous gastric cancer cells with high metastatic potential to peritoneum or lymph nodes, Cancer Res. 61 (2001) 889–895.
[15] Y. Maehara, Y. Emi, H. Baba, Y. Adachi, K. Akazawa, Y. Ichiyoshi, K. Sugimachi, Recurrences and related characteristics of gastric cancer, Br. J. Cancer 74 (1996) 975–979.
[16] A. Hagiwara, T. Takahashi, K. Sawai, C. Sakakura, M. Shirasu, M. Ohgaki, T. Imanishi, J. Yamasaki, Y. Takemoto, N. Kageyama, Selective drug delivery to peri-tumoral region and regional lymphatics by local injection of aclarubicin adsorbed on activated carbon particles in patients with breast cancer—a pilot study, Anticancer Drugs 8 (1997) 666–670.
[17] C. Oussoren, G. Storm, Liposomes to target the lymphatics by subcutaneous administration, Adv. Drug Deliv. Rev. 50 (2001) 143–156.
[18] P. Hirnle, Targeted introduction of substances into the lymph nodes for endolymphatic therapy, in: Stanley P.L. Leong (Ed.), Cancer metastasis and the lymphovascular system: basis for rational therapy, Springer, 2007, p. 101.
[19] K. Yamagata, K. Kumagai, K. Shimizu, K. Masuo, Y. Nishida, A. Yasui, Gastrointestinal cancer metastasis and lymphogenous spread: viewpoint of animal models of lymphatic obstruction, Jpn. J. Clin. Oncol. 28 (1998) 104–106.
[20] Y. Matsumura, T. Hamaguchi, T. Ura, K. Muro, Y. Yamada, Y. Shimada, K. Shirao, T. Okusaka, H. Ueno, M. Ikeda, N. Watanabe, Phase I clinical trial and pharmacokinetic evaluation of NK911, a micelle-encapsulated doxorubicin, Br. J. Cancer 91 (2004) 1775–1781.
[21] T. Hamaguchi, K. Kato, H. Yasui, C. Morizane, M. Ikeda, H. Ueno, K. Muro, Y. Yamada, T. Okusuka, K. Shirao, Y. Shimada, H. Nakahama, Y. Matsumura, A phase I and pharmacokinetic study of NK105, a paclitaxel-incorporating micellar nanoparticle formulation, Br. J. Cancer 97 (2007) 170–176.
[22] Y. Matsumura, K. Kataoka, Preclinical and clinical studies of anticancer agent-incorporating polymer micelles, Cancer Sci. 100 (2009) 572–579.
[23] Y. Matsumura, Preclinical and clinical studies of NK012, an SN-38-incorporating polymeric micelles, which is designed based on EPR effect, Adv. Drug Deliv. Rev. 63 (2010) 184–192.
[24] R. Plummer, R.H. Wilson, H. Calvert, A.V. Boddy, M. Griffin, J. Sludden, M.J. Tilby, M. Eatock, D.G. Pearson, C.J. Ottley, Y. Matsumura, K. Kataoka, T. Nishiya, A Phase I clinical study of cisplatin-incorporated polymeric micelles (NC-6004) in patients with solid tumours, Br. J. Cancer 104 (2011) 593–598.
[25] H. Cabral, N. Nishiyama, S. Okazaki, H. Koyama, K. Kataoka, Preparation and biological properties of dichloro(1,2-diaminocyclohexane)platinum (II) (DACHPt)-loaded polymeric micelles, J. Control. Release 101 (2005) 223–232.
[26] H. Cabral, N. Nishiyama, K. Kataoka, Optimization of (1,2-diamino-cyclohexane) platinum(II)-loaded polymeric micelles directed to improved tumour targeting and enhanced antitumour activity, J. Control. Release 121 (2007) 146–155.
[27] S. Kaida, H. Cabral, M. Kumagai, A. Kishimura, Y. Terada, M. Sekino, I. Aoki, N. Nishiyama, T. Tani, K. Kataoka, Visible drug delivery by supramolecular nanocarriers directing to single-platformed diagnosis and therapy of pancreatic tumor model, Cancer Res. 70 (2010) 7031–7041.
[28] M. Murakami, H. Cabral, Y. Matsumoto, S. Wu, M.R. Kano, T. Yamori, N. Nishiyama, K. Kataoka, Improving drug potency and efficacy by nanocarrier-mediated subcellular targeting, Sci. Transl. Med. 3 (2011) 64ra2.
[29] H. Cabral, Y. Matsumoto, K. Mizuno, Q. Chen, M. Murakami, M. Kimura, Y. Terada, M.R. Kano, K. Miyazono, M. Uesaka, N. Nishiyama, K. Kataoka, Accumulation of sub-100nm polymeric micelles in poorly permeable tumours depends on size, Nat. Nanotech. 6 (2011) 815–823.
[30] T. Fujihara, T. Sawada, K. Hirakawa, Y.S. Chung, M. Yashiro, T. Inoue, M. Sowa, Establishment of lymph node metastatic model for human gastric cancer in nude mice and analysis of factors associated with metastasis, Clin. Exp. Metastasis 16 (1998) 389–398.
[31] M. Yashiro, K. Hirakawa, Cancer–stromal interactions in scirrhous gastric carcinoma, Cancer Microenviron. 3 (2010) 127–135.
[32] K. Shibuya, J. Shirakawa, T. Kameyama, S. Honda, S. Tahara Hanaoka, A. Miyamoto, M. Onodera, T. Sumida, H. Nakauchi, H. Miyoshi, A. Shibuya, CD226 (DNAM-1) is involved in lymphocyte function-associated antigen 1 costimulatory signal for naive T cell differentiation and proliferation, J. Exp. Med. 198 (2003) 1829–1839.
[33] C. Iwata, M.R. Kano, A. Komuro, M. Oka, K. Kiyono, E. Johansson, Y. Morishita, M. Yashiro, K. Hirakawa, M. Kaminishi, K. Miyazono, Inhibition of cyclooxygenase-2 suppresses lymph node metastasis via reduction of lymphangiogenesis, Cancer Res. 67 (2007) 10181–10189.
[34] D.E. Jenkins, Y. Oei, Y.S. Hornig, S.F. Yu, J. Dusich, T. Purchio, P.R. Contag, Bioluminescent imaging (BLI) to improve and refine traditional murine models of tumor growth and metastasis, Clin. Exp. Metastasis. 20 (2003) 733–744.
[35] M.S. Karpeh, L. Leon, D. Klimstra, M.F. Brennan, Lymph node staging in gastric cancer: is location more important than Number? An analysis of 1,038 patients, Ann. Surg. 232 (2000) 362–371.
[36] C.Y. Chen CY, C.W. Wu, S.S. Lo, M.C. Hsieh, W.Y. Lui, K.H. Shen, Peritoneal carcinomatosis and lymph node metastasis are prognostic indicators in patients with Borrmann type IV gastric carcinoma, Hepatogastroenterology 49 (2002) 874–877.
[37] C. Oussoren, G. Storm, Lymphatic uptake and biodistribution of liposomes after subcutaneous injection: III. Influence of surface modification with poly(ethyleneglycol), Pharm. Res. 14 (1997) 1479–1484.
[38] G. Luo, X. Yu, C. Jin, F. Yang, D. Fu, J. Long, J. Xu, C. Zhan, W. Lu, LyP-1-conjugated nanoparticles for targeting drug delivery to lymphatic metastatic tumors, Int. J. Pharm. 385 (2010) 150–156.
[39] M.G. Harisinghani, J. Barentsz, P.F. Hahn, W.M. Deserno, S. Tabatabaei, C.H. van de Kaa, J. de la Rosette, R. Weissleder, Noninvasive detection of clinically occult lymph-node metastases in prostate cancer, N. Engl. J. Med. 348 (2003) 2491–2499.

Please cite this article as: M. Rafi, et al., Polymeric micelles incorporating (1,2-diaminocyclohexane)platinum (II) suppress the growth of orthotopic scirrhous gastric tumors ..., J. Control. Release (2012), doi:10.1016/j.jconrel.2012.01.038

Journal of Controlled Release 157 (2012) 112–117

Contents lists available at ScienceDirect

Journal of Controlled Release

journal homepage: www.elsevier.com/locate/jconrel

Micellization of cisplatin (NC-6004) reduces its ototoxicity in guinea pigs

Miyuki Baba [a,b], Yu Matsumoto [a,b], Akinori Kashio [a], Horacio Cabral [c], Nobuhiro Nishiyama [b], Kazunori Kataoka [b,c,d,e], Tatsuya Yamasoba [a,*]

[a] Department of Otolaryngology and Head and Neck Surgery, Faculty of Medicine, Graduate School of Medicine, Hongo 7-3-1, Bunkyo-Ku, Tokyo, 113–8655, Japan
[b] Division of Clinical Biotechnology, Center for Disease Biology and Integrative Medicine, Graduate School of Medicine, Hongo 7-3-1, Bunkyo-Ku, Tokyo, 113–8655, Japan
[c] Department of Bioengineering, Graduate School of Engineering, Hongo 7-3-1, Bunkyo-Ku, Tokyo, 113–8655, Japan
[d] Department of Materials Engineering, Graduate School of Engineering, Hongo 7-3-1, Bunkyo-Ku, Tokyo, 113–8655, Japan
[e] Center for NanoBio Integration, University of Tokyo, Hongo 7-3-1, Bunkyo-Ku, Tokyo, 113–8655, Japan

ARTICLE INFO

Article history:
Received 3 February 2011
Accepted 17 July 2011
Available online 23 July 2011

Keywords:
Auditory brainstem response
Cisplatin
Guinea pig
Hair cell
Polymeric micelle
Ototoxicity

ABSTRACT

Nanocarriers potentially reduce or prevent chemotherapy-induced side effects, facilitating the translation of nanocarrier formulation into the clinic. To date, organ-specific toxicity by nanocarriers remains to be clarified. Here, we studied the potential of polymeric micelle nanocarriers to prevent the ototoxicity, which is a common side effect of high-dose cisplatin (CDDP) therapy. In this study, we evaluated the ototoxicity of CDDP-incorporating polymeric micelles (NC-6004) in guinea pigs in comparison with that of cisplatin. Their auditory brainstem responses (ABRs) to 2, 6, 12, 20, and 30 kHz sound stimulation were measured before and 5 days after the drug administration. Groups treated with NC-6004 showed no apparent ABR threshold shifts, whereas groups treated with CDDP showed dose-dependent threshold shifts particularly at the higher frequencies. Consistent with the ABR results, groups treated with NC-6004 showed excellent hair-cell preservation, whereas groups treated with CDDP exhibited significant hair-cell loss ($P<0.05$). Synchrotron radiation-induced X-ray fluorescence spectrometry imaging demonstrated that the platinum distribution and concentration in the organ of Corti were significantly reduced ($P<0.01$) in guinea pigs treated with NC-6004 compared with guinea pigs treated with CDDP. These findings indicate that micellization of CDDP reduces its ototoxicity by circumventing the vulnerable cells in the inner ear.

1. Introduction

Recently, nanocarrier-mediated drug delivery has received great attention in cancer therapy since nanocarriers carrying chemotherapeutic agents have shown to enhance antitumor activity with reduced side effects [1–4]. The antitumor activity is enhanced because the tumor accumulation is augmented in the nanocarriers via the enhanced permeability and retention (EPR) effect [5], which is based on the following pathophysiological characteristics of solid tumors: hypervascularity, incomplete vascular architecture, secretion of vascular permeability factors stimulating extravasation within the cancer tissue, and the absence of effective lymphatic drainage. However, the reduction or prevention of chemotherapy-induced side effects, especially organ-specific toxicity, by nanocarriers remains to be completely clarified. The mechanisms of nanocarrier-mediated reduction of chemotherapy-induced organ-specific toxicity must be shown to facilitate the translation of nanocarrier formulation into the clinic.

Polymeric micelles, which are self-assemblies of block copolymers, have gained increasing popularity as nanocarriers for chemotherapeutic agents since their critical features, including size and drug loading and release, can be modulated by engineering block copolymers. Polymeric micelles carrying chemotherapeutic agents can selectively and effectively accumulate in the solid tumors, thereby leading to enhanced antitumor activity. Currently, our micelle formulations of paclitaxel (PTX), SN-38 (a biologically active metabolite of CPT-11), cisplatin (*cis*-dichlorodiammineplatinum(II), CDDP), and 1,2-diaminocyclohexane (DACHPt) are being tested in clinical trials. Regarding chemotherapy-induced side effects, polymeric micelles have been revealed to restrain the neurotoxicity of PTX and CDDP [6,7], intestinal toxicity of CPT-11 [8], and the nephrotoxicity of CDDP [7].

CDDP is a common chemotherapeutic agent used to treat many different types of cancer, including lung, gastrointestinal, bladder, and head and neck cancer. The major dose-limiting factors in CDDP therapy is the nephrotoxicity, which can be reversed to some extent by increasing the saline hydration and by using diuretic agents. As aforementioned, micellization of CDDP can prevent the nephrotoxicity,

* Corresponding author at: Department of Otolaryngology and Head and Neck Surgery, Graduate School of Medicine, University of Tokyo, Hongo 7-3-1, Bunkyo-ku, Tokyo 113–8655, Japan. Tel.: +81 3 5800 8924; fax: +81 3 3814 9486.
E-mail address: tyamasoba-tky@umin.ac.jp (T. Yamasoba).

0168-3659/$ – see front matter © 2011 Elsevier B.V. All rights reserved.
doi:10.1016/j.jconrel.2011.07.026

thereby allowing hydration-free CDDP treatment for the improvement of the patients' QOL.

CDDP-induced hearing loss is usually bilateral, irreversible, and cumulative. Audiological studies have indicated that up to 90% of the patients receiving CDDP experience significant hearing loss, especially at high frequencies [9]. The CDDP-induced hearing loss is particularly serious in pediatric populations because loss of hearing at this developmental stage hampers speech and cognitive and social development. Therefore, there is an imperative need for developing treatments that will ameliorate CDDP-induced ototoxicity. However, to date, no such cures or preventive treatments are available. In the present study, we evaluated the ototoxicity of polymeric micelles incorporating CDDP (NC-6004) in comparison with that of CDDP. NC-6004 has been evaluated in a phase I clinical trial in the United Kingdom [10], and the phase I/II trial is now underway in East Asia.

2. Materials and Methods

2.1. Materials

CDDP was purchased from WC Heraeus GmbH & Co., KG (Hanau, Germany). NC-6004 was prepared according to the slightly modified procedure that was previously reported [11] and supplied by NanoCarrier Co. Ltd. (Chiba, Japan). In brief, NC-6004 is a polymer–metal complex micelle comprising CDDP and sodium salt of poly (ethylene glycol)–poly(glutamic acid) block copolymer [PEG-P(Glu)] [11].

2.2. Animals

We used 20 healthy male Hartley-strain albino guinea pigs (weighing 243–314 g; Saitama Experimental Animals Supply Co. Ltd., Japan) with normal Preyer's reflex. The animals were housed, 5 together, in animal cages and given free access to food and water. A 12-hour dark-light cycle was maintained. They were anesthetized with a mixture of ketamine hydrochloride (40 mg/kg; Daiichi Sankyo Prophama Co. Ltd., Japan) and xylazine hydrochloride (10 mg/kg; Bayer Healthcare, Germany) during all measurements and intravenous injection procedures. All animal experiments conformed to the guidelines of the University Committee for the Use and Care of Animals, University of Tokyo, and the National Institutes of Health Guide for the Care and Use of Laboratory Animals.

2.3. Drug administration

The animals were divided into five groups according to the drug administered. Groups Cis(8) ($n=4$) and Cis(12) ($n=6$) received a bolus intravenous injection of 8 and 12 mg/kg CDDP, respectively, as well as 20 ml normal saline subcutaneously immediately after the injection to decrease the renal damage. Groups Cis-m(8) ($n=3$) and Cis-m(12) ($n=4$) received a bolus intravenous injection of NC-6004 comprising 8 and 12 mg/kg CDDP, respectively, but no subcutaneous hydration. The control group ($n=3$) received normal saline intravenously.

2.4. Auditory brainstem response measurement

Auditory brainstem responses (ABRs) were measured before and 5 days after the drug administration. The tympanic membranes were examined before the recording to ensure normal middle ear appearance. Needle electrodes were placed subcutaneously at the vertex (active electrode), beneath the pinna of the left ear (reference electrode), and beneath the right ear (ground electrode). The sound stimulus consisted of a 7 ms tone burst with a rise-fall time of 1 ms at 2, 6, 12, 20, and 30 kHz. The ABRs to 500 sweeps were averaged at each intensity level (5 dB steps) to assess the threshold, which was defined as the lowest intensity level at which a clear reproducible waveform is visible in the trace. When an ABR waveform could not be evoked, the threshold was assumed to be 5 dB greater than the maximum intensity produced by the system (105 dB sound pressure level). Threshold shifts were calculated by subtracting the pre-administration thresholds from the post-administration thresholds.

2.5. Hair-cell count

The animals in groups Cis(12) and Cis-m(12) were sacrificed under deep anesthesia after the ABR measurements and their left temporal bone was removed. The cochleae were harvested from the temporal bone and perfused with 4% paraformaldehyde in 0.1 M phosphate buffer (PFA) through a perforation in the apex and the opened oval window. They were postfixed in 4% PFA overnight and stored at 4 °C. PFA was removed by rinsing the samples in phosphate-buffered saline (PBS). The lateral wall, tectorial membrane, and Reissner's membrane were removed, and the cochlear sensory epithelium was detached from the bony shell. The epithelial cells were permeabilized in 0.3% Triton X-100 in PBS for 10 min, rinsed in PBS, stained with 1% rhodamine-phalloidin (Sigma Chemical Co., St. Louis, MO, USA) for 40 min, and once again rinsed in PBS. The organ of Corti was separated from the modiolus and mounted on glass slides. Surface preparation assessment was performed under confocal microscopy (LSM 510 META, Carl Zeiss, Inc., Jena, Germany). The total numbers of hair cells and damaged hair cells were counted from the apex to the basal turn. For the analysis of each cochlea, the whole length of the basilar membrane except the hook was assessed. A cytocochleogram was prepared by plotting the mean percentage of missing hair cells as a function of the percentage length of the organ of Corti.

2.6. Platinum distribution and concentration measurement

Synchrotron radiation-induced X-ray fluorescence spectrometry (μSR-XRF) imaging was performed to determine the platinum distribution in sections of the organ of Corti from groups Cis(12) and Cis-m(12). The left temporal bone was removed, surface preparation of the organ of Corti was performed as mentioned in the preceding, and the samples were fixed on polypropylene sheets. μSR-XRF was performed by using beam line 37XU at SPring-8 (Hyogo, Japan), at 8 GeV and about 100 mA. A photon beam with energy of 14 keV, a beam-spot size of $1.3\times1.3\ \mu m^2$, and intensity of 10^{12} photons/s was irradiated on the tissue samples. The fluorescence X-rays were measured by using a Si-SSD (Silicon solid state detector) in air at room temperature. The samples on the acryl board were then mounted on an x–y translation stage. The fluorescence X-ray intensity was normalized to the incident X-ray intensity, I_0, to produce a two-dimensional elemental map. Tissue sections of $250\times250\ \mu m^2$ were roughly scanned before the imaging. The count of platinum atoms in the samples was converted to the concentration of platinum by using the calibration standards (10 and 500 μM) of CDDP. The total intensity per tissue area was determined by using ImageJ 1.43u software (US National Institutes of Health).

2.7. Statistical analysis

We used SigmaStat software (Systat Software, Inc., Chicago, IL, USA) for statistical analysis. The ABR threshold shifts at each frequency were compared among the control and experimental groups. Bartlett's test was used to test the normality of the distribution, and one-way analysis of variance (ANOVA), Tukey–Kramer or Kruskal–Wallis test, or Dunn's test was used according to the distribution. The survival rates of the inner and outer hair cells in groups Cis(12) and Cis-m(12) were compared by using a two-tailed Student's t-test. A value of $P<0.05$ was considered statistically

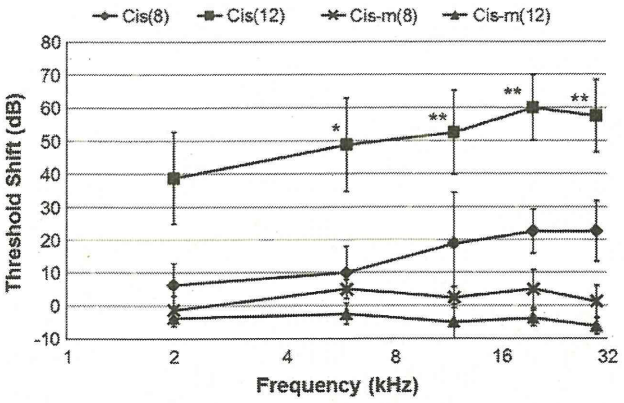

Fig. 1. ABR threshold shifts from the baseline to five days after drug administration. All results represent the mean ± SEM. *$P<0.05$, **$P<0.01$.

significant. The data were calculated as the mean ± standard error of the mean (SEM).

3. Results

Two animals in group Cis(12) died within four days of the 12 mg/kg CDDP administration (33% mortality), and were thus excluded from the data analysis. The LD_{50} for a single injection of CDDP is 9.7 mg/kg in guinea pigs [12].

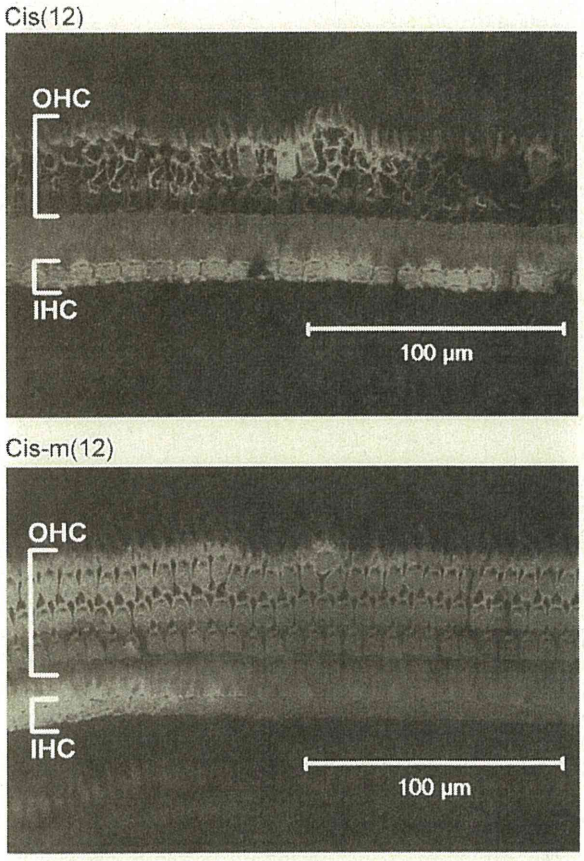

Fig. 2. Representative rhodamine-phalloidin-stained sections of the organ of Corti in the basal turn in groups Cis(12) (left) and Cis-m(12) (right). Three rows of the outer hair cells (OHCs) and a single row of the inner hair cells (IHCs) are well preserved in an animal treated with Cis-m(12), whereas almost all of the OHCs and a few IHCs are missing in an animal treated with Cis(12).

3.1. ABR threshold shifts

The ABR threshold shifts of the experimental groups are shown in Fig. 1. Group Cis(8) showed mild ABR threshold shifts (range = 6–23 dB) at the measured frequencies, but group Cis(12) demonstrated larger shifts (range = 39–60 dB) that were more severely affected by the higher frequencies. In contrast, groups Cis-m(8) and Cis-m(12) showed virtually no ABR threshold shifts. The Cis(8) ABR thresholds tended to be more affected than the Cis-m(8) ABR thresholds, although the differences between the groups were not statistically significant. Groups Cis(12) and Cis-m(12) had significant differences at all frequencies ($P<0.05$ at 2 kHz and $P<0.01$ at 6, 12, 20, and 30 kHz).

3.2. Hair-cell survival rates

In the normal organ of Corti, 3 rows of the outer hair cells (OHCs) and a single row of the inner hair cells (IHCs) can be observed. Fig. 2 shows the representative rhodamine-phalloidin-stained organ of Corti in the basal turn in groups Cis(12) and Cis-m(12). Significant damage of the OHCs and mild damage of the IHCs were observed in group Cis(12), whereas only few notable damages were observed in both the IHCs and OHCs in group Cis-m(12).

In terms of the IHC survival rates (Fig. 3A), approximately 10% of the IHCs were lost in group Cis(12) group, whereas less than 3% of these hair cells were lost in group Cis-m(12). Between the groups, significant differences in the IHC survival rate were noted at the distances of 30%, 40%, 70%, and 80% from the apex ($P<0.05$). The difference was also significant when the total IHC loss was compared ($P<0.05$).

Fig. 3B shows the survival rates of the OHCs in groups Cis(12) and Cis-m(12). Approximately 50% of these hair cells were lost in group Cis(12), whereas less than 15% were lost in group Cis-m(12). In group Cis(12), the extent of OHC loss ranged from 21% at 10% from the apex to 68% at 80% from the apex, indicating that the basal region was more severely affected than the apical region. Comparatively, the animals in group Cis-m(12) showed less damage in the OHCs, but similarly, the basal region was more severely affected than the apical region: the extent of OHC loss was less than 20% in all the segments except 90% from the apex (25% loss). These groups showed significant differences in the OHC survival rates at the distances of 20%, 40%, and 60–90% from the apex ($P<0.05$). The difference was also significant when the total OHC loss was compared ($P<0.05$).

3.3. Platinum distribution and concentration

Fig. 4 shows the platinum distribution in the organ of Corti in groups Cis(12) and Cis-m(12). Group Cis(12) had an apparently higher platinum concentration in the organ of Corti than group Cis-m(12). The mean intensity of platinum per tissue area of the organ of Corti (count/mm^2) was significantly greater in group Cis(12) than in group Cis-m(12) ($P<0.01$; Table 1).

4. Discussion

The main targets of CDDP in the cochlea are the OHCs in the organ of Corti and the stria vascularis, the vascularized epithelium in the cochlear lateral wall [13]. CDDP induces a caspase-dependent apoptotic pathway in these sensitive cochlear cells [14]. The molecular mechanisms that trigger apoptosis in the cochlea have not been elucidated, but several mechanisms have been proposed, such as increased generation of reactive oxygen species [13,15]. Platinum analogs, such as carboplatin [16] and oxaliplatin [17], have been developed to overcome the CDDP-related side effects. However, clinical trials have shown that the regimens including CDDP are still the most useful platinum-containing antineoplastic drugs [18]. Dozens of experimental studies have attempted to find ideal protective agents

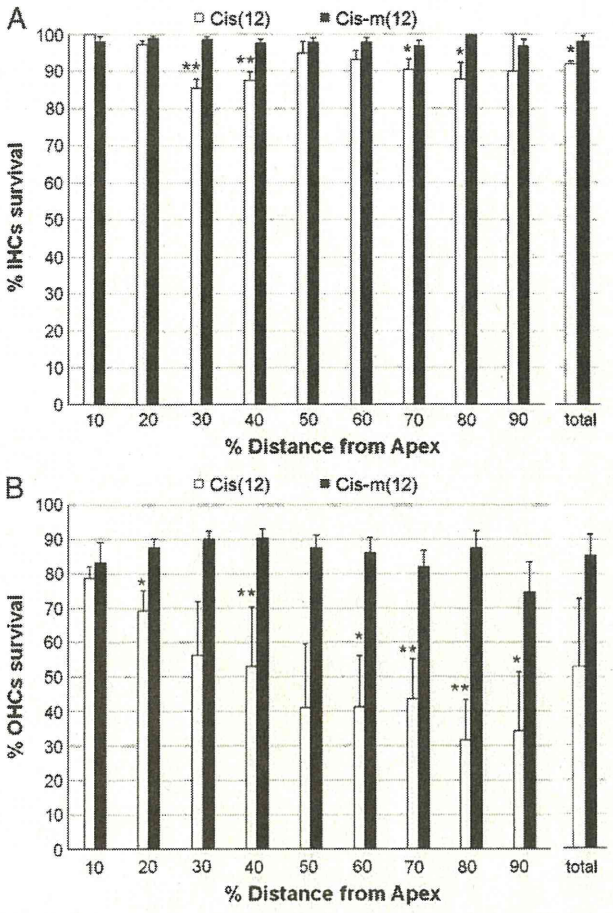

Fig. 3. Survival rates of the inner and outer hair cells in groups Cis(12) and Cis-m(12) determined five days after drug administration by using cytocochleograms. The survival rates of the inner (A) and outer (B) hair cells were calculated as percentages of the number of surviving hair cells in the experimental groups to that in the control group in each field. The results represent the mean ± SEM ($n = 4$ guinea pigs in each group). $^{*}P<0.05$, $^{**}P<0.01$.

against CDDP ototoxicity. Previous studies have shown that antioxidants, including sodium thiosulfate [19], D- or L-methionine [20,21], diethyldithiocarbamate [22,23], lipoic acid [24], and N-acetylcysteine [25], are useful in scavenging reactive oxygen species in the inner ear. However, systemic administration of L-methionine or sodium thiosulfate may inactive CDDP and reduces its antitumor activity. To prevent CDDP ototoxicity without reducing its antitumor activity, these agents require invasive approaches for delivery into the inner ear. Several other agents that protect from CDDP ototoxicity and also preserve its antitumor effect have been developed; round window application of adenosine A1 receptor agonists [26,27] and oral administration of ebselen and allopurinol [28], sodium butyrate [29], and salicylates [30] are partially effective in reducing CDDP ototoxicity without affecting its antitumor activity in animals. Until now, however, no clinical interventions have been shown to prevent CDDP ototoxicity and ensure safe therapy without reduced antitumor activity [31]. The development of a drug-delivery technology offering better selective accumulation of CDDP in solid tumors while lessening its distribution in normal tissues is therefore anticipated.

In this study, we evaluated the ototoxicity of NC-6004 and CDDP, and found that the animals given NC-6004 intravenously showed virtually no ABR threshold shifts, excellent inner and outer hair-cell preservation, and reduced platinum distribution and concentration in the organ of Corti compared with those that received the same doses of cisplatin. These results clearly indicate the markedly less-extensive ototoxicity of NC-6004.

The organ of Corti is isolated from the systemic circulation by the blood–cochlear barrier, which is similar to the blood–brain barrier [32]. CDDP readily penetrates this barrier and enters the perilymph of the inner ear, where it reaches the hair cells and exerts its toxic action. The limited cochlear uptake of oxaliplatin is considered responsible for the lower ototoxicity of oxaliplatin than CDDP [33]. The particle size of NC-6004 is approximately 30 nm [11] and that of the intrastrial space is approximately 15 nm [33,34]; therefore, the decreased ototoxicity of NC-6004 is mainly attributable to its circumvention of the IHCs and OHCs by not crossing the stria vascularis, which forms a part of the blood–cochlear barrier.

In the current study, the differences in the platinum distribution between animals treated with CDDP and NC-6004 were elucidated by

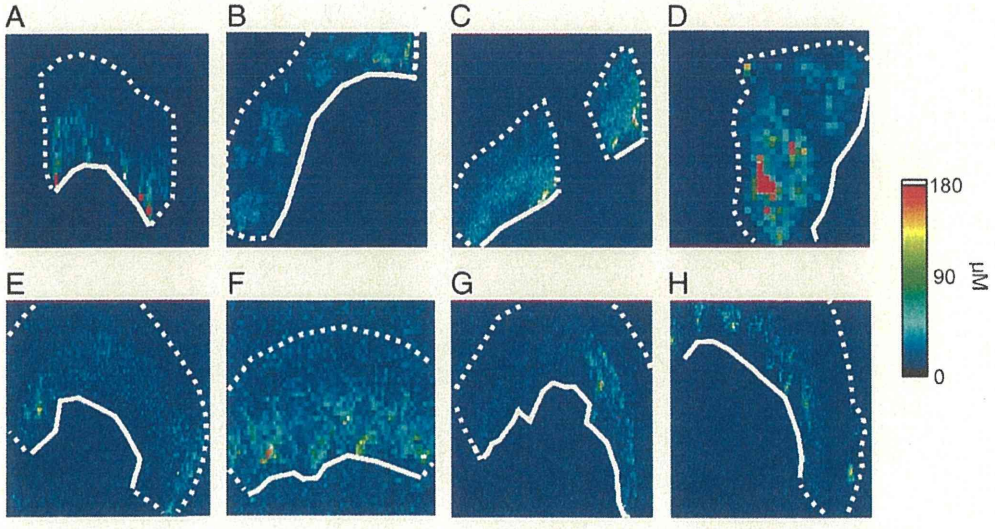

Fig. 4. Synchrotron radiation-induced X-ray fluorescence spectrometry images of the platinum distribution and concentration in the organ of Corti. The white lines indicate the basilar membrane and the areas surrounded by the broken lines indicate the presence of platinum. The cochlear epithelium in groups (A–D) Cis(12) and (E–H) Cis-m(12) at distances of approximately 20%, 40%, 60%, and 80% from the apex are shown.

Table 1
The mean intensity of platinum per tissue area (count/mm^2) shown in Fig. 4.

Group	Figure	Tissue area intensity	Background intensity	Tissue area-to-background intensity ratio
Cis(12)	A	22.06	3.39	6.51
Cis(12)	B	6.55	0.95	6.93
Cis(12)	C	21.99	3.85	5.72
Cis(12)	D	67.68	10.07	6.72
Average				6.47
Cis-m(12)	E	6.92	4.29	1.61
Cis-m(12)	F	48.81	33.63	1.45
Cis-m(12)	G	10.27	5.79	1.77
Cis-m(12)	H	8.92	5.39	1.65
Average				1.62

The data were rounded off to the second decimal place.

μSR-XRF. Until now, 2 sampling techniques have been used to measure the platinum concentration in the cochlea: sampling of the perilymph in the scala tympani [33] and homogenizing the cochlear tissue [35]. In either of the techniques, it is impossible to measure the platinum concentration only in the organ of Corti. In contrast, μSR-XRF enables (semi-)quantitative measurement of platinum concentration in the organ of Corti. The limitation of our technique is that its resolution is not high enough to distinguish each cell in the organ of Corti, which contains not only the hair cells but also the supporting cells. Thus, we could not measure the platinum concentration exclusively in the hair cells, one of the main targets of CDDP-induced cell damage. However, a previous immunohistochemical study [36], in which the CDDP was detected indirectly in the guinea pig cochlea by using an antiserum containing antibodies against CDDP-DNA adducts, showed that, while platinated DNA was present in the nuclei of most cells in the organ of Corti after CDDP administration, the nuclei of the OHCs exhibited prominent immunostaining, with the nuclei of all other (supporting) cells being only weakly stained. Therefore, it is reasonable that the platinum concentration in the organ of Corti measured by μSR-XRF is mainly derived from the OHCs.

Reportedly, there is a large difference in the CDDP concentration between the perilymph and the blood, and ABR threshold shifts are related to the CDDP concentration in the blood but not in the perilymph [37]. These findings suggest that a high plasma concentration of CDDP could collapse the blood–cochlear barrier at the initial stage after CDDP administration. NC-6004 is a long-circulating carrier with a gradual-release profile of CDDP [11]. Therefore, the reduced ototoxicity of NC-6004 can also be explained by the possibility that the gradual-release profile of CDDP from NC-6004 avoids an abrupt transient increase in the plasma CDDP concentration at the initial stage after its administration, thereby preserving the blood–cochlear barrier. This view is consistent with the fact that NC-6004 has negligible nephrotoxicity compared with CDDP, which shows a transient increase in its initial blood concentration [7]. There is also a significant correlation between the plasma creatinine level, an indicator of renal function, and the concentration of platinum [38]. Therefore, the reduced nephrotoxicity of NC-6004 might contribute to its reduced ototoxicity.

5. Conclusion

The present study demonstrated that the systemic administration of CDDP induced dose-dependent ABR threshold shifts and hair cell damage in guinea pigs, whereas such adverse effects were virtually absent after the systemic administration of NC-6004. The μSR-XRF imaging showed that the platinum distribution in the organ of Corti was significantly reduced by the micellization of CDDP. These findings confirm that the micellization of CDDP reduces its ototoxicity without additional administration of protective agents, and these findings have not been reported in previous studies. This advantage will improve patient compliance in cancer chemotherapy while maintaining substantial antitumor efficacy.

Acknowledgements

This research was supported by the Funding Program for World-Leading Innovative R&D on Science and Technology (FIRST Program) of the Japan Society for the Promotion of Science (JSPS) (to K.K.), the Core Research Program for Evolutional Science and Technology (CREST) of the Japan Science and Technology Corporation (JST) (to K.K.), and Grants-in-Aid for Scientific Research from the Japanese Ministry of Education, Culture, Sports, Science and Technology (to Y.M. and T.Y.).

References

[1] P.A. Vasey, S.B. Kaye, R. Morrison, C. Twelves, P. Wilson, R. Duncan, A.H. Thomson, L.S. Murray, T.E. Hilditch, T. Murray, S. Burtles, D. Fraier, E. Frigerio, J. Cassidy, Phase I clinical and pharmacokinetic study of PK1 [N-(2-hydroxypropyl) methacrylamide copolymer doxorubicin]: first member of a new class of chemotherapeutic agents-drug-polymer conjugates. Cancer Research Campaign Phase I/II Committee, Clin. Cancer Res. 5 (1999) 83–94.
[2] T. Lian, R.J. Ho, Trends and developments in liposome drug delivery systems, J. Pharm. Sci. 90 (2001) 667–680.
[3] M.E. Davis, Z.G. Chen, D.M. Shin, Nanoparticle therapeutics: an emerging treatment modality for cancer, Nat. Rev. Drug Discov. 7 (2008) 771–782.
[4] M. Orditura, F. Quaglia, F. Morgillo, E. Martinelli, E. Lieto, G. De Rosa, D. Comunale, M.R. Diadema, F. Ciardiello, G. Catalano, F. De Vita, Pegylated liposomal doxorubicin: pharmacologic and clinical evidence of potent antitumor activity with reduced anthracycline-induced cardiotoxicity (review), Oncol. Rep. 12 (2004) 549–556.
[5] Y. Matsumura, H. Maeda, A new concept for macromolecular therapeutics in cancer chemotherapy: mechanism of tumoritropic accumulation of proteins and the antitumor agent smancs, Cancer Res. 46 (1986) 6387–6392.
[6] T. Hamaguchi, Y. Matsumura, M. Suzuki, K. Shimizu, R. Goda, I. Nakamura, I. Nakatomi, M. Yokoyama, K. Kataoka, T. Kakizoe, NK105, a paclitaxel-incorporating micellar nanoparticle formulation, can extend in vivo antitumour activity and reduce the neurotoxicity of paclitaxel, Br. J. Cancer 92 (2005) 1240–1246.
[7] H. Uchino, Y. Matsumura, T. Negishi, F. Koizumi, T. Hayashi, T. Honda, N. Nishiyama, K. Kataoka, S. Naito, T. Kakizoe, Cisplatin-incorporating polymeric micelles (NC-6004) can reduce nephrotoxicity and neurotoxicity of cisplatin in rats, Br. J. Cancer 93 (2005) 678–687.
[8] Y. Matsumura, Preclinical and clinical studies of NK012, an SN-38-incorporating polymeric micelles, which is designed based on EPR effect, Adv. Drug Deliv. Rev. 63 (2011) 184–192.
[9] L. Helson, E. Okonkwo, L. Anton, E. Cvitkovic, cis-Platinum ototoxicity, Clin. Toxicol. 13 (1978) 469–478.
[10] R. Plummer, R.H. Wilson, H. Calvert, A.V. Boddy, M. Griffin, J. Sludden, M.J. Tilby, M. Eatock, D.G. Pearson, C.J. Ottley, Y. Matsumura, K. Kataoka, T. Nishiya, A Phase I clinical study of cisplatin-incorporated polymeric micelles (NC-6004) in patients with solid tumours, Br. J. Cancer 104 (2011) 593–598.
[11] N. Nishiyama, S. Okazaki, H. Cabral, M. Miyamoto, Y. Kato, Y. Sugiyama, K. Nishio, Y. Matsumura, K. Kataoka, Novel cisplatin-incorporated polymeric micelles can eradicate solid tumors in mice, Cancer Res. 63 (2003) 8977–8983.
[12] R.W. Fleischman, S.W. Stadnicki, M.F. Ethier, U. Schaeppi, Ototoxicity of cis-dichlorodiammine platinum (II) in the guinea pig, Toxicol. Appl. Pharmacol. 33 (1975) 320–332.
[13] L.P. Rybak, C.A. Whitworth, D. Mukherjea, V. Ramkumar, Mechanisms of cisplatin-induced ototoxicity and prevention, Hear. Res. 226 (2007) 157–167.
[14] A. Forge, L. Li, Apoptotic death of hair cells in mammalian vestibular sensory epithelia, Hear. Res. 139 (2000) 97–115.
[15] N. Dehne, J. Lautermann, F. Petrat, U. Rauen, H. de Groot, Cisplatin ototoxicity: involvement of iron and enhanced formation of superoxide anion radicals, Toxicol. Appl. Pharmacol. 174 (2001) 27–34.
[16] M. Wake, S. Takeno, D. Ibrahim, R. Harrison, Selective inner hair cell ototoxicity induced by carboplatin, Laryngoscope 104 (1994) 488–493.
[17] C.A. Rabik, M.E. Dolan, Molecular mechanisms of resistance and toxicity associated with platinating agents, Cancer Treat. Rev. 33 (2007) 9–23.
[18] J. Lokich, What is the "best" platinum: cisplatin, carboplatin, or oxaliplatin? Cancer Invest. 19 (2001) 756–760.
[19] W.C. Otto, R.D. Brown, L. Gage-White, S. Kupetz, M. Anniko, J.E. Penny, C.M. Henley, Effects of cisplatin and thiosulfate upon auditory brainstem responses of guinea pigs, Hear. Res. 35 (1988) 79–85.
[20] K.C. Campbell, L.P. Rybak, R.P. Meech, L. Hughes, D-methionine provides excellent protection from cisplatin ototoxicity in the rat, Hear. Res. 102 (1996) 90–98.
[21] D. Reser, M. Rho, D. Dewan, L. Herbst, G. Li, H. Stupak, K. Zur, J. Romaine, D. Frenz, L. Goldbloom, R. Kopke, J. Arezzo, T. Van De Water, L- and D- methionine provide equivalent long term protection against CDDP-induced ototoxicity in vivo, with partial in vitro and in vivo retention of antineoplastic activity, Neurotoxicology 20 (1999) 731–748.
[22] M.W. Church, J.A. Kaltenbach, B.W. Blakley, D.L. Burgio, The comparative effects of sodium thiosulfate, diethyldithiocarbamate, fosfomycin and WR-2721 on ameliorating cisplatin-induced ototoxicity, Hear. Res. 86 (1995) 195–203.

[23] L.P. Rybak, K. Husain, C. Morris, C. Whitworth, S. Somani, Effect of protective agents against cisplatin ototoxicity, Am. J. Otol. 21 (2000) 513–520.
[24] L.P. Rybak, K. Husain, C. Whitworth, S.M. Somani, Dose dependent protection by lipoic acid against cisplatin-induced ototoxicity in rats: antioxidant defense system, Toxicol. Sci. 47 (1999) 195–202.
[25] D. Thomas Dickey, L.L. Muldoon, D.F. Kraemer, E.A. Neuwelt, Protection against cisplatin-induced ototoxicity by N-acetylcysteine in a rat model, Hear. Res. 193 (2004) 25–30.
[26] M.S. Ford, S.B. Maggirwar, L.P. Rybak, C. Whitworth, V. Ramkumar, Expression and function of adenosine receptors in the chinchilla cochlea, Hear. Res. 105 (1997) 130–140.
[27] C.A. Whitworth, V. Ramkumar, B. Jones, N. Tsukasaki, L.P. Rybak, Protection against cisplatin ototoxicity by adenosine agonists, Biochem. Pharmacol. 67 (2004) 1801–1807.
[28] E.D. Lynch, R. Gu, C. Pierce, J. Kil, Combined oral delivery of ebselen and allopurinol reduces multiple cisplatin toxicities in rat breast and ovarian cancer models while enhancing anti-tumor activity, Anticancer Drugs 16 (2005) 569–579.
[29] M. Drottar, M.C. Liberman, R.R. Ratan, D.W. Roberson, The histone deacetylase inhibitor sodium butyrate protects against cisplatin-induced hearing loss in guinea pigs, Laryngoscope 116 (2006) 292–296.
[30] G. Li, S.H. Sha, E. Zotova, J. Arezzo, T. Van de Water, J. Schacht, Salicylate protects hearing and kidney function from cisplatin toxicity without compromising its oncolytic action, Lab Invest. 82 (2002) 585–596.
[31] G.W. Hill, D.K. Morest, K. Parham, Cisplatin-induced ototoxicity: effect of intratympanic dexamethasone injections, Otol. Neurotol. 29 (2008) 1005–1011.
[32] V. Hellberg, I. Wallin, S. Eriksson, E. Hernlund, E. Jerremalm, M. Berndtsson, S. Eksborg, E.S. Arnér, M. Shoshan, H. Ehrsson, G. Laurell, Cisplatin and oxaliplatin toxicity: importance of cochlear kinetics as a determinant for ototoxicity, J. Natl. Cancer Inst. 101 (2009) 37–47.
[33] S.S. Spicer, B.A. Schulte, Novel structures in marginal and intermediate cells presumably relate to functions of apical versus basal strial strata, Hear. Res. 200 (2005) 87–101.
[34] H. Hibino, Y. Kurachi, Molecular and physiological bases of the K+ circulation in the mammalian inner ear, Physiology (Bethesda) 21 (2006) 336–345.
[35] R. Ramírez-Camacho, D.E. Fernández, J.M. Verdaguer, M.M. Gómez, A. Trinidad, J.R. García-Berrocal, M.A. Corvillo, Cisplatin-induced hearing loss does not correlate with intracellular platinum concentration, Acta Otolaryngol. 128 (2008) 505–509.
[36] M.W. van Ruijven, J.C. de Groot, F. Hendriksen, G.F. Smoorenburg, Immunohistochemical detection of platinated DNA in the cochlea of cisplatin-treated guinea pigs, Hear. Res. 203 (2005) 112–121.
[37] J.W. Sepmeijer, S.F. Klis, Distribution of platinum in blood and perilymph in relation to cisplatin induced ototoxicity in the guinea pig, Hear. Res. 247 (2009) 34–39.
[38] C. Lanvers-Kaminsky, B. Krefeld, A.G. Dinnesen, D. Deuster, E. Seifert, G. Würthwein, U. Jaehde, A.C. Pieck, J. Boos, Continuous or repeated prolonged cisplatin infusions in children: a prospective study on ototoxicity, platinum concentrations, and standard serum parameters, Pediatr. Blood Cancer 47 (2006) 183–193.

ACCOUNTS
of chemical research

Supramolecular Nanodevices: From Design Validation to Theranostic Nanomedicine

HORACIO CABRAL,[†] NOBUHIRO NISHIYAMA,[‡] AND KAZUNORI KATAOKA*,[†,‡,§]

[†]*Department of Bioengineering, Graduate School of Engineering, The University of Tokyo, 7-3-1 Hongo, Bunkyo-ku, Tokyo 113-8656, Japan,* [‡]*Center for Disease Biology and Integrative Medicine, Graduate School of Medicine, The University of Tokyo, 7-3-1 Hongo, Bunkyo-ku, Tokyo 113-0033, Japan, and* [§]*Department of Materials Engineering, Graduate School of Engineering, The University of Tokyo, 7-3-1 Hongo, Bunkyo-ku, Tokyo 113-8656, Japan*

RECEIVED ON MARCH 28, 2011

CONSPECTUS

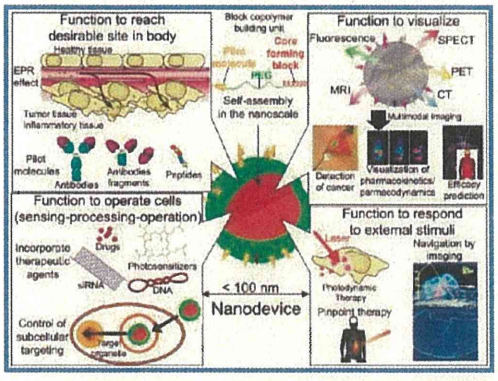

The increasing importance of nanotechnology in the biomedical field and the recent progress of nanomedicines into clinical testing have spurred the development of even more sophisticated nanoscale drug carriers. Current nanocarriers can successfully target cells, release their cargo in response to stimuli, and selectively deliver drugs. More sophisticated nanoscale carriers should evolve into fully integrated vehicles with more complex capabilities. First, they should be able to sense targets inside the body and adapt their functions based on these targets. Such devices will also have processing capabilities, modulating their properties and functions in response to internal or external stimuli. Finally, they will direct their function to the aimed site through both subcellular targeting and delivery of loaded drugs. These nanoscale, multifunctional drug carriers are defined here as nanodevices. Through the integration of various imaging elements into their design, the nanodevices can be made visible, which is an essential feature for the validation. The visualization of nanodevices also facilitates their use in the clinic: clinicians can observe the effectiveness of the devices and gain insights into both the disease progression and the therapeutic response. Nanodevices with this dual diagnostic and therapeutic function are called theranostic nanodevices.

In this Account, we describe various challenges to be overcome in the development of smart nanodevices based on supramolecular assemblies of engineered block copolymers. In particular, we focus on polymeric micelles. Polymeric micelles have recently received considerable attention as a promising vehicle for drug delivery, and researchers are currently investigating several micellar formulations in preclinical and clinical studies. By engineering the constituent block copolymers to produce polymeric micelles that integrate multiple smart functionalities, we and other researchers are developing nanodevices with favorable clinical properties.

Introduction

In the past two decades, enormous effort has been devoted to the development of nanoscale carriers that selectively deliver bioactive substances to diseased sites such as malignant cancers.[1−6] Nanoscale carriers can maximize the therapeutic efficacy and minimize the side effects of loaded drugs. Particularly, subhundred-nanometer-scale vehicles are known to accumulate selectively in solid

Published on the Web 07/14/2011 www.pubs.acs.org/accounts
10.1021/ar200094a

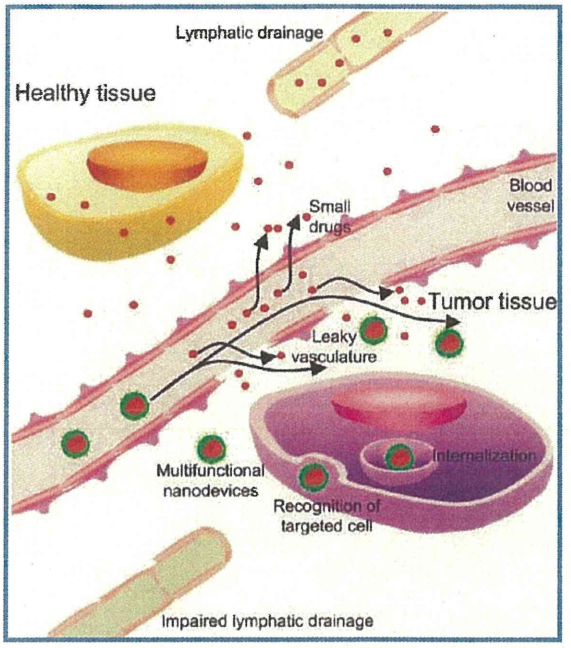

FIGURE 1. Enhanced permeability and retention (EPR) effect. Neovasculature of tumors differs greatly from that of normal tissues. Endothelial cells in tumor blood vessels are poorly aligned or disorganized with large fenestrations, causing macromolecules to leak extensively into the tumor tissue. In addition, slow venous return in the tumor tissue and poor lymphatic clearance cause macromolecules to be retained in the tumor. This effect does not apply to low-molecular-weight drugs because of their diffusion into the entire body and rapid renal clearance.

tumors due to vascular hyperpermeability and impaired lymphatic drainage,[1−6] which is termed the enhanced permeability and retention (EPR) effect (Figure 1).[7] Indeed, several nanoscale carrier formulations such as Doxil and Abraxane are already in clinical use.[8−11]

Today, nanoscale carriers can successfully achieve cellular targeting, programmable release of their cargo and selective delivery of the drugs.[1−6] Their evolution into nanodevices will rely on the consistent integration of the following multiple functions: (1) sensing (detecting targets inside the body and adapting their function based on these targets), (2) processing (modulating their properties and functions responding to internal or external stimuli), and (3) operation (properly performing the desired task in a spatiotemporally controlled manner in the body). Such nanodevices can be embodied by the "bottom-up" approach through nanoscale integration of functional components such as therapeutic and imaging agents, synthetic polymers and peptides and proteins. Considering viruses as an utmost natural example, self-assembly is an efficient process taking advantage of nature's way for construction of smart nanodevices. Nanodevices are a key platform to innovate on the existing methodologies of not only clinical diagnosis and therapy but also drug development and basic life sciences.

Imaging function can be integrated into the multifunctionality of nanodevices. The modalities for imaging include optical imaging, computed tomography (CT), ultrasound (US), magnetic resonance imaging (MRI), and nuclear imaging including single photon emission computed tomography (SPECT) and positron emission tomography (PET). Such imaging function provides the methodologies to appropriately evaluate in vivo performances of nanodevices, which are designed to exert multiple smart functions (i.e., sensing, processing and operation) in the body. In this regard, recent advances in intravital imaging technologies such as in vivo confocal microscopy facilitates in situ evaluation of nanodevices.[12,13] Thus, integration of an imaging function into nanodevices can validate the design strategy of multifunctional nanodevices, which should be essential to their optimization and further functionalization for in vivo applications. From the clinical standpoint, nanodevices with imaging function can enhance the visibility of specific tissues by increasing the signal-to-noise ratio relative to the surrounding tissues, offering ultrasensitive diagnosis against small lesions, which are undetectable by current diagnostic methods. The incorporation of different contrast agents into nanodevices enables multimodal imaging that can improve the precision of diagnosis by exploiting advantages of each imaging modality.[14,15] Furthermore, increasing attention has recently been paid to functional imaging to detect specific environments (e.g., acidic pH conditions in solid tumors), cellular responses (e.g., proliferation and apoptosis), and chemical reactions (e.g., enzymatic reactions), allowing for evaluating biological responses to specific treatments.[16,17]

In this Account, we describe the challenges in the development of more sophisticated nanodevices based on supramolecular assemblies of engineered block copolymers and discuss the concept and significance of theranostic nanodevices. In particular, we focus on polymeric micelles with core−shell architecture as practical platforms for integrating multiple functionalities.[4−6] Polymeric micelles possess ideal properties to be used as drug carriers, such as prolonged blood circulation and enhanced accumulation in solid tumors, and several micelle formulations incorporating anticancer agents have advanced to clinical studies.[18,19]

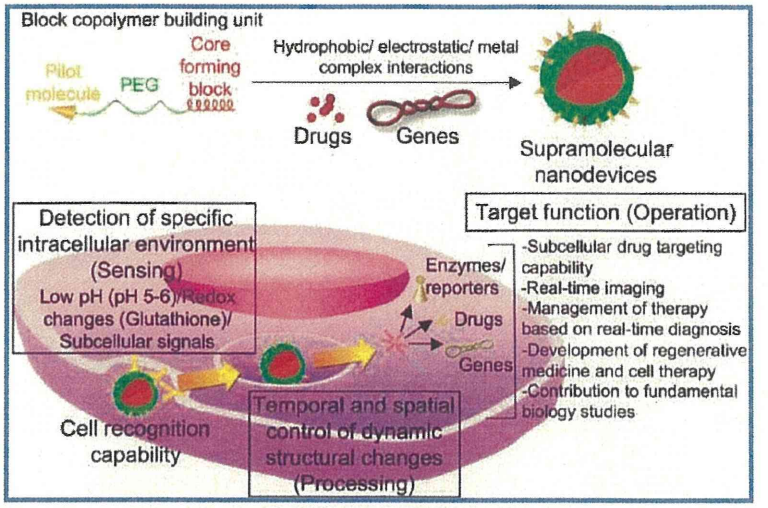

FIGURE 2. Supramolecular nanodevices as a versatile platform for cell therapy. Nanodevices can be designed to perform three functions: (1) sense specific intracellular environments; (2) process (modulate their properties and functions) responding to internal or external stimuli; and (3) operate properly at the desired site.

Integration of Functional Imaging into the Design of State-of-the-Art Nanodevices

The integration of multiple smart functions into a nanodevice platform can improve targeting to diseased sites and enhance diagnostic and therapeutic efficacies (Figure 2). These nanodevices can be designed to reach desirable sites in the body by introducing pilot molecules on their surface in addition to the control of their physicochemical parameters including size, surface charge, and stability.[1−6] Also, nanodevices are aimed to control the subcellular distribution of delivered drugs and to activate the drugs in an environmentally sensitive or external-stimuli-responsive manner.[1−6] Furthermore, nanodevices are expected to efficiently deliver plasmid DNA and siRNA to the target organelles in the cell and act as a safe and efficient nonviral vector.[20,21] Despite these advances, however, it remains controversial whether multifunctional nanodevices actually work as designed inside the body. Integrating an imaging function into the nanodevice design can enable researchers to address this uncertainty by performing in vivo evaluation of nanodevice performance, thus validating design strategies as well as facilitating optimization and further functionalization.

Recent advances in imaging technologies to assist in in vivo validation of nanodevices include whole-body imaging systems and in vivo confocal microscopy. Whole-body luminescent and near-infrared fluorescent imaging enable researchers to follow, in real time, the biodistribution of nanodevices,[22,23] validate targets,[24−26] identify subcellular trafficking pathways,[27] determine mechanisms of action, and monitor disease progression in living animals.[28,29] To enable visualization of whole-body distribution and bioavailability, nanodevices can be labeled with fluorescent dyes and quantum dots[30,31] and equipped with near-infrared probes for deep tissue imaging using contrast enhancement.[32] Intravital confocal microscopy provides instant histopathology at the cellular and subcellular levels and therefore is ideal for investigating dynamic events under in vivo conditions.[12,13,33] The technique can be used to visualize the distribution and clearance of nanodevices within various tissues and organs (Figure 3A) and is particularly effective for investigating dynamic and complex events such as blood circulation, site-specific drug accumulation, subcellular trafficking, and overcoming of biological barriers.[12] Moreover, the biological features of nanodevices can be observed in a straightforward manner. For example, direct visualization of the dynamic behavior of DNA polyplexes during circulation has demonstrated that PEGylation prevents the formation of aggregates of DNA polyplexes and their subsequent interaction with platelets (Figure 3B).[13]

Nanodevices that respond to chemical and physical stimuli to achieve intracellular drug delivery are of particular recent interest.[1−6] The stimuli-responsive controlled release of their drug payload maximizes the specificity of drug action at the target site. Furthermore, stimuli-responsive nanodevices can enhance the pharmacological activity of the loaded drugs by improving pharmacokinetics at the subcellular level. It has been reported that nanodevices designed to release active drugs in acidic organelles, such as endosomes and lysosomes, might circumvent recognition by the drug efflux pump (e.g., P-glycoprotein) through

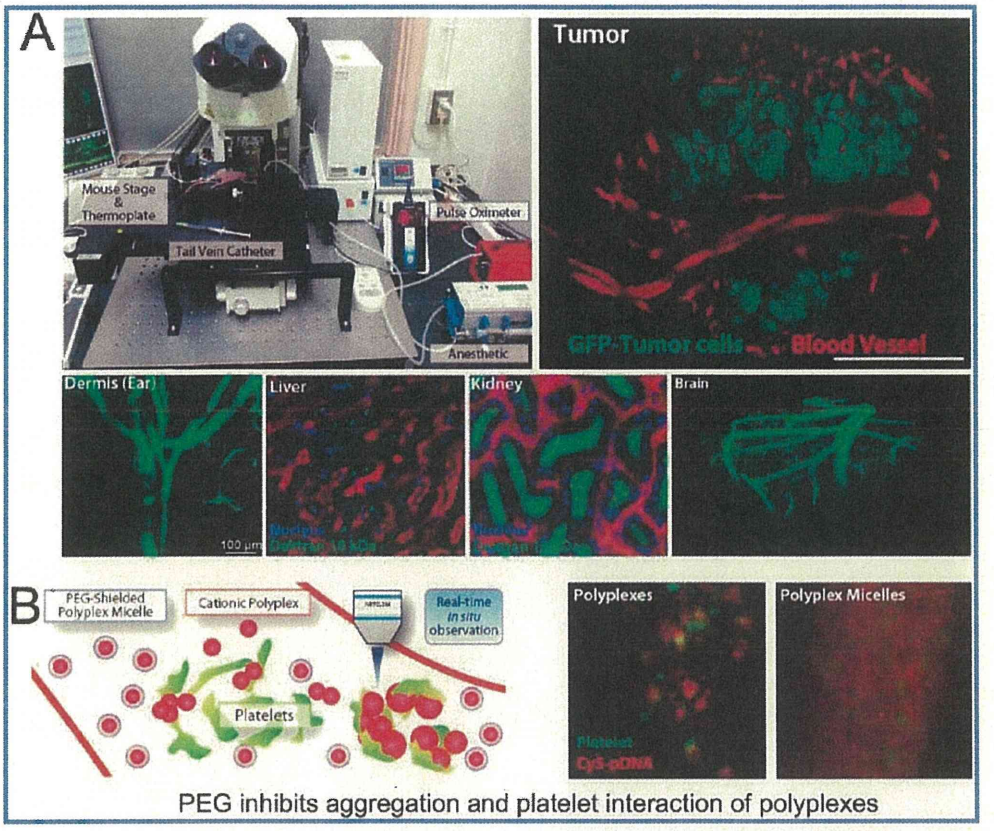

FIGURE 3. Visualization by in vivo laser confocal microscopy. (A) Scheme of in vivo laser confocal microscopy. The technique permits dynamic visualization of fluorescent molecules and biological markers at subcellular levels in tumors and healthy tissues such as ear lobe dermis, liver, kidney, or brain. Reprinted with permission from ref 12. Copyright 2010 Optical Society of America. (B) Effect of the PEGylation of DNA polyplexes observed by in vivo laser confocal microscopy. The formation of aggregates of polyplexes (red) followed by the interaction of these aggregates with platelets (green) and the prevention of these issue by PEGylation were observed in situ under the flow in a capillary. Reprinted with permission from ref 13. Copyright 2011 Elsevier.

internalization by endocytosis, thus overcoming multidrug resistance in cancer cells.[34,35]

Recently, we demonstrated that nanodevices can work as nanoscale Trojan horses to bypass drug-inactivation pathways in the cytoplasm and deliver drugs efficiently to the target nuclei, overcoming drug-resistance in cancer cells. Polymeric micelles incorporating (1,2-diaminocyclohexane)platinum(II) (DACHPt), the parent complex of anticancer drug oxaliplatin, are formed by reversible complex formation between DACHPt and poly(ethylene glycol)-*b*-poly(glutamic acid) [PEG-*b*-P(Glu)].[29,33,36] This reversible chelation allows the release of DACHPt from the micelles via ligand-substitution reaction of Pt(II) from carboxylate to chloride ion, and the release rate depends on pH and $[Cl^-]$.[29,33,36] Accordingly, DACHPt-loaded micelles accelerate DACHPt release in the late endosomal environment close to the perinuclear region because of a decrease in pH and an increase in $[Cl^-]$ following initial uptake into the early endosome.[33] Importantly, in vitro and in vivo studies revealed that DACHPt-loaded micelles showed remarkable antitumor activity against oxaliplatin-resistant tumors (Figure 4A). We hypothesized that DACHPt-loaded micelles may overcome the drug resistance by circumventing cytoplasmic detoxification systems that are activated in the drug-resistant cancer cells, as illustrated in Figure 4B. To prove this hypothesis in tumors in living animals, dual fluorescent-labeled micelles were constructed by using BODIPY FL–PEG-*b*-P(Glu)–BODIPY TR (Figure 4C). Intact micelles fluoresce only from the shell-conjugated dye BODIPY FL; the core-conjugated dye BODIPY TR concentrates in the core of the micelles and becomes quenched. As DACHPt is released from the micelles, dequenching of BODIPY TR occurs and the micelles fluoresce increasingly from BODIPY TR. Thus, dual-fluorescent labeling, using both BODIPY FL and BODIPY TR, enables researchers to determine the location of the micelles and the location of drug release that accompanies micelle dissociation (Figure 4C). Observation of the dual fluorescent-labeled micelles by intravital confocal microscopy demonstrates that while DACHPt-loaded micelles circulate stably in the bloodstream even after 12 h (Figure 4D), the micelles

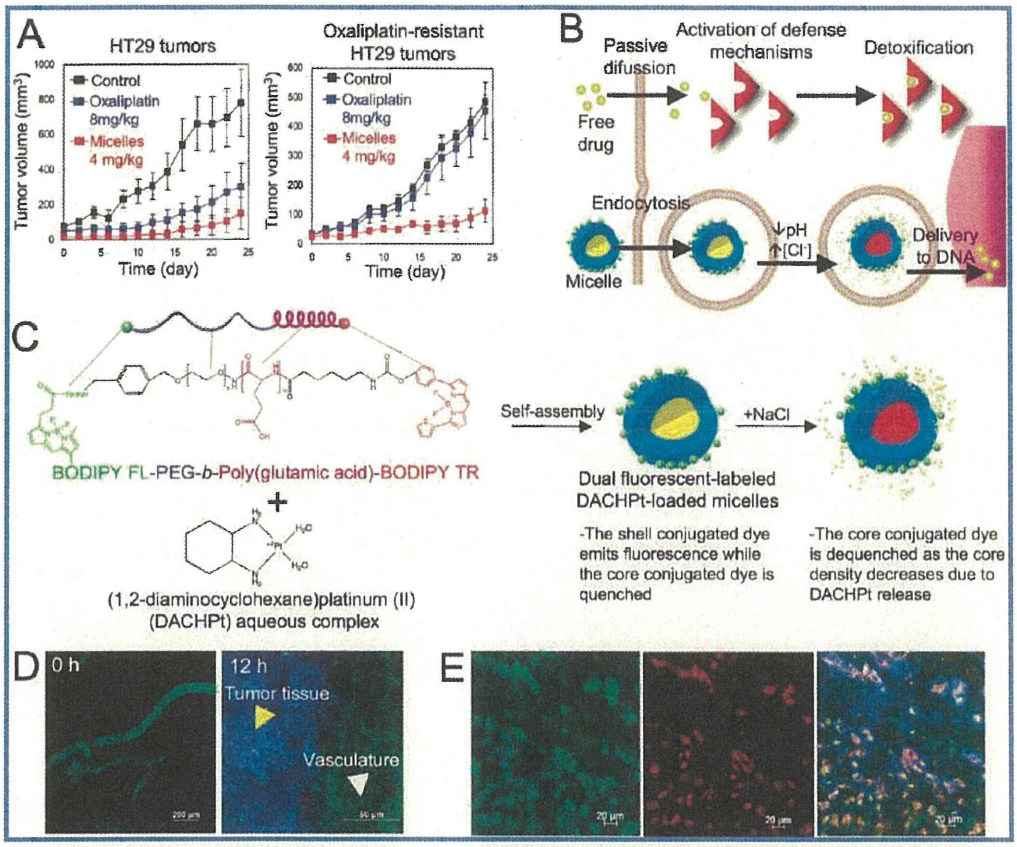

FIGURE 4. Intravital imaging of dual fluorescent-labeled DACHPt-loaded micelles for validation of the concept of intracellular drug delivery in living animals. (A) Antitumor activity of DACHPt-loaded micelles against parent and oxaliplatin-resistant human colon adenocarcinoma HT29 tumor models. The micelles overcame drug resistance in vivo. (B) Proposed mechanism by which DACHPt-loaded micelles overcome drug resistance. (C) Design of dual fluorescent-labeled DACHPt-loaded micelles for visualization of the localization and drug release in the cell. The micelles self-assemble via polymer–metal complex formation between DACHPt and BODIPY FL–poly(ethylene glycol)-*b*-poly(glutamic acid)–BODIPY TR in distilled water. In the micelle state, only BODIPY FL (green) fluoresces and BODIPY TR (red) remains quenched. As DACHPt is released from the micelles in chloride-ion-containing media, BODIPY TR becomes dequenched and begins to fluoresce. (D) In vivo confocal microscopy of micelles in blood vessels and tumor tissue after intravenous administration: immediately after injection and at 12 h after injection. These results suggest that micelles circulate stably in the bloodstream even after 12 h. (E) In vivo confocal microscopy of micelles in tumor tissues at 12 h after injection. Both green and red fluorescence are observed inside the cells, suggesting that the micelles might selectively release DACHPt inside tumor cells. Colors are as follows: green = fluorescence from the shell-conjugated dye BODIPY FL; red = fluorescence from the core-conjugated dye BODIPY TR; blue = fluorescence from the cell membrane (CellMask). Reprinted with permission from ref 33. Copyright 2011 American Association for the Advancement of Science. The merged image on the right shows the colocalization of green and red fluorescence in each cell colored blue, demonstrating subcellular DACHPt delivery by the micellar nanodevice.

penetrate deeply into cancerous tissues after extravasation, internalize into cancer cells distant from the blood vessels, and eventually dissociate and release active drugs selectively in the late endosome of cancer cells (Figure 4E).[33] Thus, the imaging functionality allowed us to validate our hypothesis that DACHPt-loaded micelles can overcome drug resistance through circumvention of the detoxification systems in the cytoplasm.

Further advances in spatial and temporal control of therapeutic effects become possible with external triggering. Externally triggerable nanodevices can enable detection of the target through the contrast-enhanced imaging, followed by pinpoint application of external stimuli to the target site for executing operating functions. Light-triggered nanodevices are attracting increasing attention due to their spatial and temporal control of the therapeutic effects. Moreover, the use of near-infrared lasers and minimally invasive fiber-optic tools facilitates direct targeting of deep tissues. Light has been used to release therapeutic agents from nanodevices[37,38] and to activate agents that produce cytotoxic species.[39] Photodynamic therapy (PDT) is a light-activated treatment modality for various diseases based on the generation of reactive oxygen species (ROS) from photosensitizers by the light irradiation, leading to selective and irreversible destruction of diseased tissues.[39] The generation of heat with light

TABLE 1. Imaging Modalities Used in Theranostic Nanodevices

imaging modality	benefits	limitations	examples of theranostic nanodevices
fluorescence	• easy labeling • great variety of fluorescent molecules and detection wavelengths • good spatial resolution, especially for near-infrared (NIR) light • no ionizing radiation	• clinical application is still limited. • potential incompatibility and toxicity of fluorescent probes • relevant wavelength range limited to 700–900 nm. • limited tissue penetration of light (≤2 cm)	Cy 5.5/doxorubicin(DOX) micelles,[22] Cy 5.5/Paclitaxel-loaded micelles[23]
MRI	• high spatial resolution • several contrast agents are widely used for clinical imaging • signal can be enhanced by incorporating contrast agents into nanodevices • no ionizing radiation	• low sensitivity • real-time imaging is difficult • potential toxicity	SPION/DOX micelles,[52–54] Gd-DTPA/(1,2-diaminocyclohexane)platinum(II) (DACHPt)-loaded micelles[51]
PET	• highly sensitive • functional imaging is feasible • signals from radionuclides can be quantified precisely.	• lack of spatial resolution • can give false results if chemical balances within the body are not normal • radionuclides involved have relatively short half-lives • limited accessibility	^{64}Cu/DOX liposomes[59]
SPECT	• highly sensitive • signals from radionuclides can be quantified precisely	• requires use of ionizing radiation • prolonged imaging time • low spatial resolution	^{188}Re/DOX liposomes[60]
CT	• depicts anatomical features precisely	• requires use of ionizing radiation • requires high concentrations of contrast agents • definitive diagnosis is still difficult by CT alone	iodine/DOX liposomes[61]
ultrasound	• safe • low cost • fast and simple	• microbubbles as contrast agents have relatively large size and short blood circulation • destruction of microbubbles ruptures vessel walls and causes hemolysis	microbubbles for gene and drug delivery[62,63]

illumination, that is, photothermal therapy (PTT), also allows localized treatment of diseased tissue by irradiation of photoabsorbers with near-infrared light to cause thermal damage. Nanodevices can improve the accuracy and efficiency of PDT and PTT with minimal damage to normal tissues.[40–42] Moreover, photochemical internalization (PCI), which is a concept of the light-induced cytoplasmic delivery of endocytosed macromolecules based on the photochemical disruption of endosomal membranes,[43] allow nanodevices to activate bioactive molecules such as plasmid DNA, siRNA, and proteins in a light-selective manner.[43–45]

Theranostic Nanodevices: The Emerging Concept of Personalized Nanomedicine

As described in the Introduction, the EPR effect has been widely observed in various tumor models in animals and has become a fundamental principle in carrier-based drug delivery targeted for cancer treatment. Indeed, several formulations such as Doxil and Abraxane are already in clinical use and have been demonstrated to be effective against certain cancers such as Kaposi sarcoma,[8] ovarian cancer,[9] and breast cancer.[10,11] Nevertheless, it remains unclear how effective and different the EPR effect is in different types of cancers in individual patients. For example, pancreatic cancer and diffuse-type gastric cancer (schirrous gastric cancer), which are characterized by less permeable vasculature with pericyte coverage and thick fibrosis, exhibit limited accumulation of macromolecules and particulates and are therefore likely to be intractable by conventional nanoscale carrier systems.[46]

As an approach for drug visualization, direct conjugation of imaging contrast agents to therapeutic entities was found to compromise the biodistribution and biological activity of the therapeutic entity. In contrast, integration of imaging functionality into nanoscale drug carriers does not affect

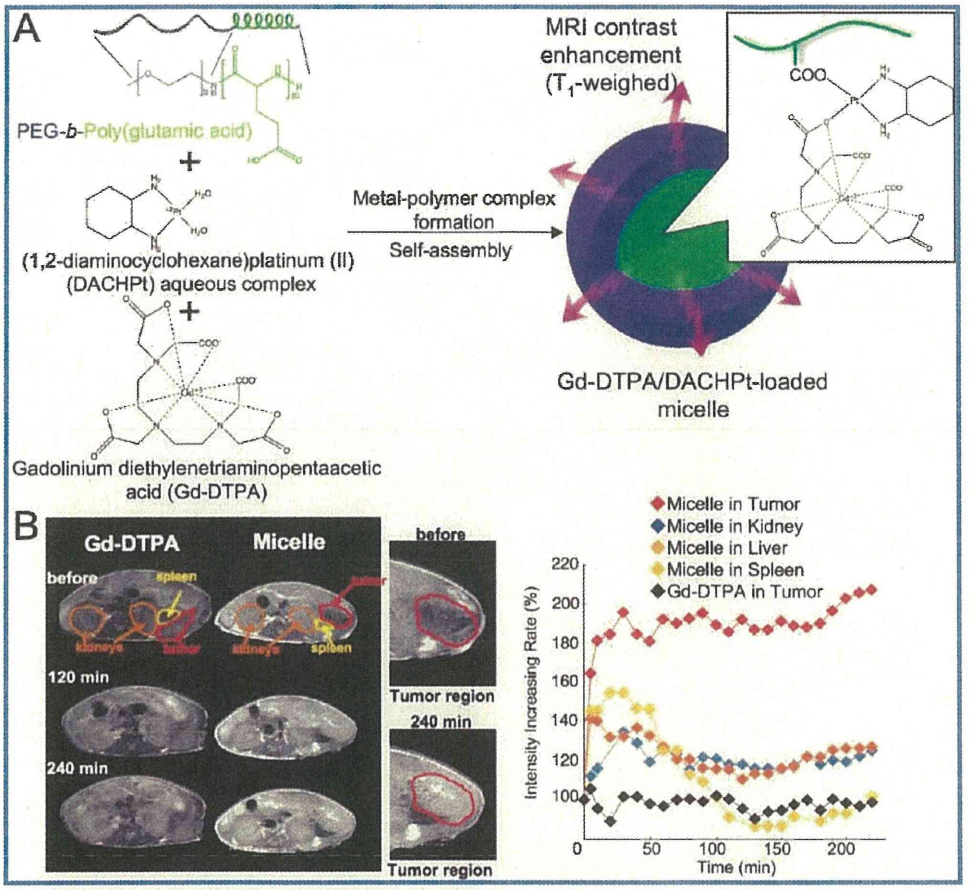

FIGURE 5. Gd–DTPA/DACHPt-loaded micelles for tracking biodistribution and therapeutic effects. (A) Scheme of Gd–DTPA/DACHPt-loaded micelles formation. Micelles self-assemble by metal-complex formation between DACHPt and the carboxylic groups of poly(glutamic acid) in PEG-*b*-P(Glu). (B) MRI of orthotopic pancreatic tumor bearing mice after intravenous injection of the clinically approved MRI contrast agent, Gd–DTPA, or Gd–DTPA/DACHPt-loaded micelles. The micelles specifically enhance the signal at the tumor site for a prolonged time. Reprinted with permission from ref 51. Copyright 2010 American Association for Cancer Research.

biodistribution and biological activity and thus offers a promising theranostic platform. Almost all imaging modalities have been used in theranostic nanodevices, and imaging has successfully provided information about anatomic distribution, pharmacokinetics, and pharmacodynamics of nanodevices and delivered drugs (Table 1). Among these imaging modalities, MRI is particularly advantageous because it offers good spatial resolution in the entire body and good contrast among soft tissues, making it especially useful for imaging muscle, brain, heart, and tumors. The basis for a MRI signal is the precession of water hydrogen nuclei in an applied magnetic field and MRI contrast agents can be used to shorten the relaxation times of water (spin–lattice relaxation time T_1 and spin–spin relaxation time T_2); contrast agents with higher relaxivities [r_1 (= $1/T_1$) and r_2 (= $1/T_2$)] give stronger contrast enhancement.[47] Paramagnetic molecules such as gadolinium (Gd) and manganese (Mn) for T_1-weighted MRI[48–51] and superparamagnetic contrast agents such as iron-oxide nanoparticles for T_2-weighted MRI[52–54] have been incorporated into nanodevices to enable tracing of tissue distribution.

Regarding T_1-enhanced contrast agents, their relaxivity is influenced by numerous parameters. Efforts to increase the relaxivity of Gd contrast agents have focused on three approaches: increasing the hydration number, optimizing the water-exchange rate, and slowing molecular reorientation.[47] However, increasing the hydration number of Gd complexes reduces their plasma stability, and optimizing the water-exchange rate requires direct engineering on the Gd complex; hence, the most practical of these approaches is to slow molecular reorientation.

One strategy to slow molecular reorientation is to decrease the mobility of Gd complexes by incorporating them into micelles, thus forming supramolecular structures with increased relaxivities.[48–50] We recently incorporated

gadolinium–diethylenetriaminepentaacetic acid (Gd–DTPA), a clinically approved T_1-weighted MRI contrast agent into DACHPt-loaded micelles by utilizing the reversible complex formation between DACHPt and Gd–DTPA (Figure 5A).[51] Incorporation of Gd–DTPA into the micellar core increases longitudinal relaxivity r_1 from 3.5 to 80.5 mmol L^{-1} s^{-1}. Gd–DTPA/DACHPt-loaded micelles released less toxic Gd–DTPA under a physiological condition, followed by its rapid renal clearance, avoiding problems of toxicity caused by long-term accumulation of Gd^{3+} ions in the body. In animal experiments, Gd–DTPA/DACHPt-loaded micelles accumulated effectively in subcutaneous murine colon carcinoma and orthotopic human pancreatic adenocarcinoma models, enabling successful contrast-enhanced MR imaging of those tumors (Figure 5B). In addition to real-time observation of tumor accumulation, contrast-enhanced MRI using Gd–DTPA/DACHPt-loaded micelles also enables the measurement of the volume of orthotopic pancreatic tumors in the abdominal cavity and, thus, noninvasive evaluation of their enhanced antitumor activity compared with free oxaliplatin. Because clinical chemotherapy regimens are given in periodic cycles over weeks or months, monitoring of tumor size by MRI using Gd–DTPA/DACHPt-loaded micelles is clinically feasible.

Regarding T_2-enhanced contrast agents, aggregation of magnetic nanoparticles dephases the spins of neighboring water protons efficiently, enhancing the net rate r_2 of transverse relaxation. The value of T_2 for a magnetic nanoparticle is inversely proportional to its cross-sectional area, so the same amount of magnetized material is more effective when dispersed as fewer large aggregates than as more smaller aggregates.[55] Accordingly, clustering superparamagnetic iron-oxide nanoparticles (SPIONs) inside polymeric micelles prepared from poly(ethylene glycol)-*block*-poly(D,L-lactide) augments their relaxivity.[52] Relaxivity enhancement of PEGylated SPIONs incorporating Dox was critical for the evaluation of their tumor accumulation by MRI.[53,54]

At present, therapeutic strategies are evaluated through population-based studies or randomized clinical trials, neither of which considers individual differences among patients. In contrast, theranostic nanodevices may enable the evaluation of real-time therapeutic responses in individual patients. They may also facilitate evaluation by enabling medical clinicians to monitor pharmacokinetic and therapeutic responses, perhaps in lieu of detecting traditional end points such as tumor shrinkage. Furthermore, theranostic nanodevices with integrated functional imaging may provide pinpoint information regarding cellular responses and biomarker expression within diseased tissues, which can be used in combination with current serum biomarkers. Nevertheless, for theranostic nanodevices to be deemed suitable for clinical use, designers must surmount the challenges involving formulation toxicity, stability under in vivo conditions, inconsistencies in the clearance rates of imaging and therapeutic agents, optimization of the dosage needed for therapy and diagnosis, and, of course, regulatory definition and acceptance. If these challenges can be surmounted, this emerging approach will likely become a safe and efficient strategy for disease management.

Prospects for the Future

Nanodevices must grow substantially in sophistication before we can experience focused smart nanomedicines in which a single platform executes seamless processes ranging from ultrasensitive diagnosis to pinpoint therapy. Integration of the imaging function into nanodevice designs provides tools for assessing nanodevice biodistribution and other functions. To date, nanodevices have been mostly applied to diagnosis and treatment of cancers, because they can selectively and effectively accumulate in cancerous tissues due to the EPR effect. For further applications of nanodevices to organs and tissues other than cancer, nanodevices need to be equipped with the capabilities to overcome several biological barriers, including extravasation, tissue penetration, and cellular internalization at the target site. Especially, the extravasation in specific tissues should be the first critical barrier. In this regard, recent advances in in vivo phage-display techniques have led to the discovery of peptides specific to the vascular endothelium in particular organs and tissues (vascular mapping),[56] motivating researchers to develop nanodevices that actively target specific peptides. Targeting vascular endothelium can increase nanodevice accumulation at the target site (tissue-specific delivery) and also facilitate nanodevice transport across the vascular wall (transcytosis), even in tissues where the EPR effect does not operate to cause accumulation.[57,58] Actively targetable nanodevices can potentially overcome other formidable biological barriers as well, such as the blood-brain barrier. Among promising directions of investigation, nanodevices will eventually permit in situ detection and manipulation of the expression of specific molecules, molecular interactions, and reactions, providing new tools for the direct study of molecular and cellular biological events in living animals. Such sophisticated nanodevices

should be useful for drug discovery and development based on validation of molecular targets by whole-body imaging.

Medical nanodevices will continue to evolve by capitalizing on advances in related fields such as drug delivery, materials science, molecular imaging, molecular and cellular biology, and clinical oncology, as well as on technical improvements for assessment of nanodevices. Multidisciplinary approaches resulting from collaborations among researchers from various fields are clearly indispensable to this evolution and the realization of innovative nanodevices.

BIOGRAPHICAL INFORMATION

Horacio Cabral received his Ph.D. under the supervision of Prof. K. Kataoka in Materials Engineering from the University of Tokyo in 2007. He worked as an assistant professor at the Division of Clinical Biotechnology, Graduate School of Medicine, the University of Tokyo until 2009. Since 2010, he has been an associate professor at the Department of Bioengineering, the University of Tokyo. His main research interests relate to smart nanodevices for the diagnosis and therapy of cancer.

Nobuhiro Nishiyama received his Ph.D. under the supervision of Prof. K. Kataoka in Materials Engineering from the University of Tokyo in 2001. After a postdoctoral fellowship in the research group of Professor J. Kopecek at the University of Utah, he joined in the research group of Prof. K. Kataoka again in 2003 and has been an associate professor in the Division of Clinical Biotechnology, Graduate School of Medicine, the University of Tokyo since 2009. His main interest concerns the biomedical applications of intelligent nanodevices for drug and gene delivery.

Kazunori Kataoka received his Ph.D. from the University of Tokyo in 1979. He has been a professor of Biomaterials at Graduate School of Engineering, the University of Tokyo, Japan since 1998. He has also been appointed a joint position since 2004 from Graduate School of Medicine, the University of Tokyo as a professor of Clinical Biotechnology. Dr. Kataoka is the author of more than 380 scientific papers in international journals and is on the board of 14 internationally renowned scientific journals. His current major research interests include the development of new polymeric carrier systems, especially block copolymer micelles, for drug and gene targeting.

The research in this Account was supported in part by Funding Program for World-Leading Innovative R&D on Science and Technology (FIRST Program) from the Japan Society for the Promotion of Science (JSPS).

FOOTNOTES

*To whom correspondence should be addressed. Telephone: +81-3-5841-7109. Fax: +81-3-5841-7139. E-mail: kataoka@bmw.t.u-tokyo.ac.jp.

REFERENCES

1 Duncan, R. The dawning era of polymer therapeutics. *Nat. Rev. Drug Discovery* **2003**, *2*, 347–360.

2 Ferrari, M. Cancer nanotechnology: opportunities and challenges. *Nat. Rev. Cancer* **2005**, *5*, 161–171.

3 Davis, M. E.; Chen, Z.; Shin, D. Nanoparticle therapeutics: an emerging treatment modality for cancer. *Nat. Rev. Drug Discovery* **2008**, *7*, 771–782.

4 Kataoka, K.; Harada, A.; Nagasaki, Y. Block copolymer micelles for drug delivery: design, characterization and biological significance. *Adv. Drug Delivery Rev.* **2001**, *47*, 113–131.

5 Nishiyama, N.; Kataoka, K. Current state, achievements, and future prospects of polymeric micelles as nanocarriers for drug and gene delivery. *Pharmacol. & Ther.* **2006**, *112*, 630–648.

6 Cabral, H.; Kataoka, K. Multifunctional nanoassemblies of block copolymers for future cancer therapy. *Sci. Technol. Adv. Mater.* **2010**, *11*, 014109.

7 Matsumura, Y.; Maeda, H. A new concept for macromolecular therapeutics in cancer chemotherapy: mechanism of tumouritropic accumulation of proteins and the antitumour agent SMANCS. *Cancer Res.* **1986**, *46*, 6387–6392.

8 Northfelt, D. W.; Dezube, B. J.; Thommes, J. A.; Miller, B. J.; Fischl, M. A.; Friedman-Kien, A.; Kaplan, L. D.; Du Mond, C.; Mamelok, R. D.; Henry, D. H. Pegylated-liposomal doxorubicin versus doxorubicin, bleomycin, and vincristine in the treatment of AIDS-related Kaposi's sarcoma: results of a randomized phase III clinical trial. *J. Clin. Oncol.* **1998**, *16*, 2445–2451.

9 Gordona, A. N.; Tondab, M.; Sunc, S.; Rackoff, W. Long-term survival advantage for women treated with pegylated liposomal doxorubicin compared with topotecan in a phase 3 randomized study of recurrent and refractory epithelial ovarian cancer. *Gynecol. Oncol.* **2004**, *95*, 1–8.

10 O'Brien, M. E. R.; Wigler, N.; Inbar, M.; Rosso, R.; Grischke, E.; Santoro, A.; Catane, R.; Kieback, D. G.; Tomczak, P.; Ackland, S. P.; Orlandi, F.; Mellars, L.; Alland, L.; Tendler, C. Reduced cardiotoxicity and comparable efficacy in a phase III trial of pegylated liposomal doxorubicin HCl (CAELYX/Doxil) versus conventional doxorubicin for first-line treatment of metastatic breast cancer. *Ann. Oncol.* **2004**, *15*, 440–449.

11 Gradishar, W. J.; Tjulandin, S.; Davidson, N.; Shaw, H.; Desai, N.; Bhar, P.; Hawkins, M.; O'Shaughnessy, J. Phase III trial of nanoparticle albumin-bound paclitaxel compared with polyethylated castor oil-based paclitaxel in women with breast cancer. *J. Clin. Oncol.* **2005**, *23*, 7794–7803.

12 Matsumoto, Y.; Nomoto, T.; Cabral, H.; Matsumoto, Y.; Watanabe, S.; Christie, J.; Miyata, K.; Oba, M.; Ogra, T.; Yamasaki, Y.; Nishiyama, N.; Yamasoba, T.; Kataoka, K. Direct and instantaneous observation of intravenously injected substances using intravital confocal micro-videography. *Biomed. Opt. Express* **2010**, *1*, 1209–1216.

13 Nomoto, T.; Matsumoto, Y.; Miyata, K.; Oba, M.; Fukushima, S.; Nishiyama, N.; Yamasoba, T.; Kataoka, K. In situ quantitative monitoring of polyplexes and polyplex micelles in the blood circulation using intravital real-time confocal laser scanning microscopy. *J. Controlled Release* **2011**, *151*, 104–109.

14 Cheon, J.; Lee, J.-H. Synergistically integrated nanoparticles as multimodal probes for nanobiotechnology. *Acc. Chem. Res.* **2008**, *41*, 1630–1640.

15 Janib, S. M.; Moses, A. S.; MacKay, J. A. Imaging and drug delivery using theranostic nanoparticles. *Adv. Drug Delivery Rev.* **2010**, *62*, 1052–1063.

16 Zhang, J.; Campbell, R. E.; Ting, A. Y.; Tsien, R. Creating new fluorescent probed for cell biology. *Nat. Rev. Mol. Cell Biol.* **2002**, *3*, 906–918.

17 Kobayashi, H.; Choyke, P. L. Target-cancer-cell-specific activatable fluorescence imaging probes: Rational design and in vivo applications. *Acc. Chem. Res.* **2011**, *44*, 83–90.

18 Matsumura, Y.; Kataoka, K. Preclinical and clinical studies of anticancer agent-incorporating polymer micelles. *Cancer Sci.* **2009**, *100*, 572–579.

19 Plummer, R.; Wilson, R. H.; Calvert, H.; Boddy, A. V.; Griffin, M.; Sludden, J.; Tilby, M. J.; Eatock, M.; Pearson, D. G.; Ottley, C. J.; Matsumura, Y.; Kataoka, K.; Nishiya, T. A phase I clinical study of cisplatin-incorporated polymeric micelles (NC-6004) in patients with solid tumours. *Br. J. Cancer* **2011**, *104*, 593–598.

20 Mastrobattista, E.; van der Aa, M. A. E. M; Hennink, W. E.; Crommelin, D. J. A. Artificial viruses: a nanotechnological approach to gene delivery. *Nat. Rev. Drug Discovery* **2006**, *5*, 115–121.

21 Whitehead, K. A.; Langer, R.; Anderson, D. G. Knocking down barriers: advances in siRNA deliver. *Nat. Rev. Drug Discovery* **2009**, *8*, 129–138.

22 Kim, D.; Gao, Z.; Lee, E.; Bae, Y. H. In vivo evaluation of doxorubicin-loaded polymeric micelles targeting folate receptors and early endosomal pH in drug-resistant ovarian cancer. *Mol. Pharmaceutics* **2009**, *6*, 1353–1362.

23 Tsai, H.-C.; Chang, W.-H.; Lo, C.-L.; Tsai, C.-H.; Chang, C.-H.; Ou, T.-W.; Yen, T.-C.; Hsiue, G.-H. Graft and diblock copolymer multifunctional micelles for cancer chemotherapy and imaging. *Biomaterials* **2010**, *31*, 2293–2301.

24 Mahmood, U.; Weissleder, R. Near-infrared optical imaging of proteases in cancer. *Mol. Cancer Ther.* **2003**, *2*, 489–496.

25 Jaffer, F. A.; Libby, P.; Weissleder, R. Molecular and cellular imaging of atherosclerosis: emerging applications. *J. Am. Coll. Cardiol.* **2006**, *47*, 1328–1338.

26 Bullok, K.; Piwnica-Worms, D. Synthesis and characterization of a small, membrane-permeant, caspase-activatable far-red fluorescent peptide for imaging apoptosis. *J. Med. Chem.* **2005**, *48*, 5404–5407.

27 Altnoğlu, E. I.; Russin, T. J.; Kaiser, J. M.; Barth, B. M.; Eklund, P. C.; Kester, M.; Adair, J. H. Near-infrared emitting fluorophore-doped calcium phosphate nanoparticles for in vivo imaging of human breast cancer. *ACS Nano* **2008**, *2*, 2075–2084.

28 Itaka, K.; Osada, K.; Morii, K.; Kim, P.; Yun, S.-H.; Kataoka, K. Polyplex nanomicelle promotes hydrodynamic gene introduction to skeletal muscle. *J. Controlled Release* **2010**, *143*, 112–119.

29 Cabral, H.; Nishiyama, N.; Kataoka, K.. Optimization of (1,2-diamino-cyclohexane)platinum(II)-loaded polymeric micelles directed to improved tumor targeting and enhanced antitumor activity. *J. Controlled Release* **2007**, *121*, 146–155.

30 He, X.; Wang, K.; Cheng, Z. In vivo near-infrared fluorescence imaging of cancer with nanoparticle-based probes. *Wiley Interdiscip. Rev.: Nanomed. Nanobiotechnol.* **2010**, *2*, 349–366.

31 Michalet, X.; Pinaud, F. F.; Bentolila, L. A.; Tsay, J. M.; Doose, S. J.; Li, J.; Sundaresan, G.; Wu, A. M.; Gambhir, S. S.; Weiss, S. Quantum dots for live cells, in vivo imaging, and diagnostics. *Science* **2005**, *307*, 538–544.

32 Weissleder, R. A clearer vision for in vivo imaging. *Nat. Biotechnol.* **2001**, *19*, 316–317.

33 Murakami, M.; Cabral, H.; Matsumoto, Y.; Wu, S.; Kano, M. R.; Yamori, T.; Nishiyama, N.; Kataoka, K. Improving drug potency and efficacy by nanocarrier-mediated subcellular targeting. *Sci. Transl. Med.* **2011**, *3*, 64ra2.

34 Minko, T.; Kopecková, P.; Kopecek, J. Efficacy of the chemotherapeutic action of HPMA copolymer-bound doxorubicin in a solid tumor model of ovarian carcinoma. *Int. J. Cancer* **2000**, *86*, 108–117.

35 Kim, D.; Lee, E. S.; Oh, K. T.; Gao, Z. G.; Bae, Y. H. Doxorubicin-loaded polymeric micelle overcomes multidrug resistance of cancer by double-targeting folate receptor and early endosomal pH. *Small* **2008**, *4*, 2043–2050.

36 Cabral, H.; Nishiyama, N.; Okazaki, S.; Koyama, H.; Kataoka, K. Preparation and biological properties of dichloro(1,2-diaminocyclohexane)platinum(II) (DACHPt)-loaded polymeric micelles. *J. Controlled Release* **2005**, *101*, 223–232.

37 Jiang, J.; Tong, X.; Morris, D.; Zhao, Y. Toward Photocontrolled release using light-dissociable block copolymer micelles. *Macromolecules* **2006**, *39*, 4633–4640.

38 Babin, J.; Pelletier, M.; Lepage, M.; Allard, J.-F.; Morris, D.; Zhao, Y. A New Two-photon-sensitive block copolymer nanocarrier. *Angew. Chem., Int. Ed.* **2009**, *121*, 3379–3382.

39 Henderson, B.; Dougherty, T. How does photodynamic therapy work? *Photochem. Photobiol.* **1992**, *55*, 145–157.

40 Chatterjee, D. K.; Fong, L. S.; Zhang, Y. Nanoparticles in photodynamic therapy: an emerging paradigm. *Adv. Drug Delivery Rev.* **2008**, *60*, 1627–1637.

41 Nishiyama, N.; Morimoto, Y.; Jang, W.-D.; Kataoka, K. Design and development of dendrimer photosensitizer-incorporated polymeric micelles for enhanced photodynamic therapy. *Adv. Drug Delivery Rev.* **2009**, *61*, 327–338.

42 Hirsch, L. R.; Stafford, R. J.; Bankson, J. A.; Sershen, S. R.; Rivera, B.; Price, R. E.; Hazle, J. D.; Halas, N. J.; West, J. L. Nanoshell-mediated near-infrared thermal therapy of tumors under magnetic resonance guidance. *Proc. Natl. Acad. Sci. U.S.A.* **2003**, *100*, 13549–13554.

43 Berg, K.; Weyergang, A.; Prasmickaite, L.; Bonsted, A.; Høgset, A.; Strand, M. T.; Wagner, E.; Selbo, P. K. Photochemical internalization (PCI): a technology for drug delivery. *Methods Mol. Biol.* **2010**, *635*, 133–145.

44 Nishiyama, N.; Iriyama, A.; Jang, W.-D.; Miyata, K.; Itaka, K.; Inoue, Y.; Takahashi, H.; Yanagi, T.; Tamaki, Y.; Koyama, H.; Kataoka, K. Light-induced gene transfer from packaged DNA enveloped in a dendrimeric photosensitizer. *Nat. Mater.* **2005**, *4*, 934–941.

45 Cabral, H.; Nakanishi, M.; Kumagai, M.; Jang, W.-D.; Nishiyama, N.; Kataoka, K. A photo-cctivated targeting chemotherapy using glutathione sensitive camptothecin-loaded polymeric micelles. *Pharm. Res.* **2009**, *26*, 82–92.

46 Kano, M. R.; Bae, Y.; Iwata, C.; Morishita, Y.; Yashiro, M.; Oka, M.; Fujii, T.; Komuro, A.; Kiyono, K.; Kaminishi, M.; Hirakawa, K.; Ouchi, Y.; Nishiyama, N.; Kataoka, K.; Miyazono, K. Improvement of cancer-targeting therapy, using nanocarriers for intractable solid tumours by inhibition of TGF-β signalling. *Proc. Natl. Acad. Sci. U.S.A.* **2007**, *104*, 3460–3465.

47 Krause, W. *Contrast agents I: magnetic resonance imaging*; Topics in Current Chemistry 221; Springer-Verlag: Berlin, 2002.

48 Kimpe, K.; Parac-Vogt, T.; Laurent, S.; Pierart, C.; Vander Elst, L.; Muller, R. N.; Binnemans, K. Potential MRI contrast agents based on micellar incorporation of amphiphilic bis-(alkylamide) derivatives of $[(Gd\text{-}DTPA)(H_2O)]^{2-}$. *Eur. J. Inorg. Chem.* **2003**, 3021–3027.

49 Tournier, H.; Hyacinthe, R.; Schneider, M. Gadolinium-containing mixed micelle formulations: a new class of blood pool MRI/MRA contrast agents. *Acad. Radiol.* **2002**, *9*, S20–S28.

50 Anelli, P. L.; Lattuada, L.; Lorusso, V.; Schneider, M.; Tournier, H.; Uggeri, F. Mixed micelles containing lipophilic gadolinium complexes as MRI contrast agents. *Magn. Reson. Mater. Phys. Biol. Med.* **2001**, *12*, 114–120.

51 Kaida, S.; Cabral, H.; Kumagai, M.; Kishimura, A.; Terada, Y.; Sekino, M.; Aoki, I.; Nishiyama, N.; Tani, T.; Kataoka, K. Visible drug delivery by supramolecular nanocarriers directing to single-platformed diagnosis and therapy of pancreatic tumor model. *Cancer Res.* **2010**, *70*, 7031–7041.

52 Nasongkla, N.; Bey, E.; Ren, J.; Ai, H.; Khemtong, C.; Guthi, J. S.; Chin, S.-F.; Sherry, A. D.; Boothman, D. A.; Gao, J. Multifunctional polymeric micelles as cancer-targeted, MRI-ultrasensitive drug delivery systems. *Nano Lett.* **2006**, *6*, 2427–2430.

53 Lee, H.; Lee, E.; Kim, D.; Jang, N.; Jeong, Y.; Jon, S. Antibiofouling polymer-coated superparamagnetic iron oxide nanoparticles as potential magnetic resonance contrast agents for in vivo cancer imaging. *J. Am. Chem. Soc.* **2006**, *128*, 7383–7389.

54 Yu, M.; Jeong, Y.; Park, J.; Park, S.; Kim, J.; Min, J.; Kim, K.; Jon, S. Drug-loaded superparamagnetic iron oxide nanoparticles for combined cancer imaging and therapy in vivo. *Angew. Chem., Int. Ed.* **2008**, *47*, 5362–5365.

55 Gillis, P.; Koenig, S. H. Transverse relaxation of solvent protons induced by magnetized spheres: Application to ferritin, erythrocytes, and magnetite. *Magn. Res. Med.* **1987**, *5*, 323–345.

56 Arap, W.; Kolonin, M. G.; Trepel, M.; Lahdenranta, J.; Cardó-Vila, M.; Giordano, R. J.; Mintz, P. J.; Ardelt, P. U.; Yao, V. J.; Vidal, C. I.; Chen, L.; Flamm, A.; Valtanen, H.; Weavind, L. M.; Hicks, M. E.; Pollock, R. E.; Botz, G. H.; Bucana, C. D.; Koivunen, E.; Cahill, D.; Troncoso, P.; Baggerly, K. A.; Pentz, R. D.; Do, K.-A.; Logothetis, C. J.; Pasqualini, R. Steps toward mapping the human vasculature by phage display. *Nat. Med.* **2002**, *8*, 121–127.

57 McIntosh, D. P.; Tan, X.-Y.; Oh, P.; Schnitzer, J. E. Targeting endothelium and its dynamic caveolae for tissue-specific transcytosis in vivo: A pathway to overcome cell barriers to drug and gene delivery. *Proc. Natl. Acad. Sci. U.S.A.* **2002**, *99*, 1996–2001.

58 Sugahara, K. N.; Teesalu, T.; Karmali, P. P.; Kotamraju, V. R.; Agemy, L.; Girard, O. M.; Hanahan, D.; Mattrey, R. F.; Ruoslahti1, E. Tissue-penetrating delivery of compounds and nanoparticles into tumors. *Cancer Cell* **2009**, *16*, 510–520.

59 Kheirolomoom, A.; Mahakian, L. M.; Lai, C.-Y.; Lindfors, H. A.; Seo, J. W.; Paoli, E. E.; Watson, K. D.; Haynam, E. M.; Ingham, E. S.; Xing, L.; Cheng, R. H.; Borowsky, A. D.; Cardiff, R. D.; Ferrara, K. W. Copper–doxorubicin as a nanoparticle cargo retains efficacy with minimal toxicity. *Mol. Pharmaceutics* **2010**, *7*, 1948–1958.

60 Chen, M.; Chang, C.; Chang, Y.; Chen, L.; Yu, C.; Wu, Y.; Lee, W.; Yeh, C.; Lin, F.; Lee, T.; Yang, C.; Ting, G. MicroSPECT/CT Imaging and pharmacokinetics of ^{188}Re-(DXR)-liposome in human colorectal adenocarcinoma-bearing mice. *Anticancer Res.* **2010**, *30*, 65–72.

61 Karathanasis, E.; Chan, L.; Balusu, S. R.; D'Orsi, C. J.; Annapragada, A. V.; Sechopoulos, I.; Bellamkond, R. V. Multifunctional nanocarriers for mammographic quantification of tumor dosing and prognosis of breast cancer therapy. *Biomaterials* **2008**, *29*, 4815–4822.

62 Lindner, J. R. Microbubbles in medical imaging: current applications and future directions. *Nat. Rev. Drug Discovery* **2004**, *3*, 527–532.

63 Klibanov, A. L. Targeted delivery of gas-filled microspheres, contrast agents for ultrasound imaging. *Adv. Drug Delivery Rev.* **1999**, *37*, 139–157.

nature nanotechnology

ARTICLES

PUBLISHED ONLINE: 23 OCTOBER 2011 | DOI: 10.1038/NNANO.2011.166

Accumulation of sub-100 nm polymeric micelles in poorly permeable tumours depends on size

H. Cabral[1], Y. Matsumoto[2], K. Mizuno[3], Q. Chen[4], M. Murakami[2], M. Kimura[2], Y. Terada[5], M. R. Kano[6], K. Miyazono[6,7], M. Uesaka[3,7], N. Nishiyama[2,7]* and K. Kataoka[1,2,4,7]*

A major goal in cancer research is to develop carriers that can deliver drugs effectively and without side effects. Liposomal and particulate carriers with diameters of ~100 nm have been widely used to improve the distribution and tumour accumulation of cancer drugs, but so far they have only been effective for treating highly permeable tumours. Here, we compare the accumulation and effectiveness of different sizes of long-circulating, drug-loaded polymeric micelles (with diameters of 30, 50, 70 and 100 nm) in both highly and poorly permeable tumours. All the polymer micelles penetrated highly permeable tumours in mice, but only the 30 nm micelles could penetrate poorly permeable pancreatic tumours to achieve an antitumour effect. We also showed that the penetration and efficacy of the larger micelles could be enhanced by using a transforming growth factor-β inhibitor to increase the permeability of the tumours.

Targeting tumours with long-circulating nanomedicines, such as poly(ethylene glycol)-modified liposomes and polymeric micelles[1–6], is a promising strategy in systemic cancer treatment. These materials accumulate in solid tumours through the enhanced permeability and retention (EPR) effect[7], which is characterized by leaky blood vessels and an impaired lymphatic drainage in tumour tissues[7]. Compared with free drug, nanomedicines accumulate in solid tumours more easily and selectively and therefore offer better antitumour activity[8–15]. Several nanomedicines, including Doxil and Abraxane (diameters of 90 and 130 nm, respectively), have shown significant antitumour activity in highly vascularized tumours such as Kaposi's sarcoma and breast cancer, and have been approved for clinical use[16,17]. However, because Doxil and other nanomedicines with diameters larger than 100 nm have shown limited penetration and accumulation in tumours with hypovascular and hypopermeable characteristics[18–20] (such as intractable pancreatic tumours[18,20]), nanomedicines in the sub-100 nm range are now regarded as being more important in the study of tumour penetration[21,22].

Polymeric micelles (self-assemblies of block copolymers) are promising long-circulating nanomedicines[5,6,8–10] and have been widely studied in preclinical and clinical trials[13,14,23]. Clinical studies have demonstrated that polymeric micelles of poly(ethylene glycol)–*b*-poly(amino acid) copolymers incorporating paclitaxel, SN-38, doxorubicin or cisplatin drugs can reduce the toxic side effects of the loaded drugs[13,14,24,25] while maintaining appreciable antitumour efficacy. Micelles containing paclitaxel and SN-38 have been reported to reduce the size of tumours in patients with advanced cancers of the breast and pancreas[13,14]. The dense poly(ethylene glycol) (PEG) shell of the micelles prevents protein adsorption and recognition by the phagocyte system, and this prolongs blood circulation, a prerequisite for enhanced tumour accumulation based on the EPR effect. Moreover, with these micelles, the size (including those in the sub-100 nm range), stability, loading capacity and release kinetics of the drugs can be modulated by engineering the constituent block copolymers[5,6]. Here, we examine whether a series of micellar nanomedicines that have diameters less than 100 nm and that carry the potent tumoricidal agent 1,2-diaminocyclohexane-platinum(II) (DACHPt) (the parent complex of oxaliplatin) can accumulate and penetrate poorly permeable pancreatic tumours. Our results show that the size of the nanomedicines critically affects the penetration and efficacy of the drugs in the tumours. Larger micelles that could not penetrate otherwise, could penetrate once the permeability of the tumours was improved by administering a transforming growth factor-β inhibitor.

Characterization of DACHPt-loaded micelles

DACHPt-loaded micelles (DACHPt/m) were spontaneously formed from the interaction of the platinum of DACHPt and the carboxylic moieties of PEG–*b*-poly(glutamic acid) (PEG–*b*-P(Glu)) copolymer and the poly(glutamic acid) (P(Glu)) homopolymer in water (Fig. 1a)[10,26,27]. Differently sized DACHPt/m were synthesized by controlling the mixing ratio of P(Glu) from the homopolymer and the P(Glu) portion of PEG–*b*-P(Glu) (Fig. 1b). As the ratio of P(Glu) in the homopolymer and P(Glu) in the copolymer increases, the size of the micelles increases. Thus, the size of DACHPt/m ranged from 30 nm without the addition of P(Glu) homopolymer to more than 100 nm, while maintaining a narrow distribution as determined by dynamic light scattering (DLS) measurements and transmission electron microscopy (TEM) observations (Table 1 and Supplementary Fig. S1, respectively). Note that DLS measurements provide the hydrodynamic diameter of the DACHPt/m, and TEM gives the core diameter of the micelles, so the difference between the hydrodynamic diameter and the core size gives an indication of the thickness of the PEG shell of the micelles.

[1]Department of Bioengineering, Graduate School of Engineering, The University of Tokyo, 7-3-1 Hongo, Bunkyo-ku, Tokyo, 113-8656, Japan, [2]Center for Disease Biology and Integrative Medicine, Graduate School of Medicine, The University of Tokyo, 7-3-1 Hongo, Bunkyo-ku, Tokyo 113-0033, Japan, [3]Department of Nuclear Engineering and Management, Graduate School of Engineering, The University of Tokyo, 7-3-1 Hongo, Bunkyo-ku, Tokyo 113-8656, Japan, [4]Department of Materials Engineering, Graduate School of Engineering, The University of Tokyo, 7-3-1 Hongo, Bunkyo-ku, Tokyo 113-8656, Japan, [5]SPring 8, JASRI, 1-1-1 Kouto, Sayo-cho, Sayo-gun, Hyogo 679-5198, Japan, [6]Department of Molecular Pathology, Graduate School of Medicine, The University of Tokyo, 7-3-1 Hongo, Bunkyo-ku, Tokyo 113-0033, Japan, [7]Center for NanoBio Integration (CNBI), The University of Tokyo, 7-3-1 Hongo, Bunkyo-ku, Tokyo 113-8656, Japan. *e-mail: nishiyama@bmw.t.u-tokyo.ac.jp; kataoka@bmw.t.u-tokyo.ac.jp

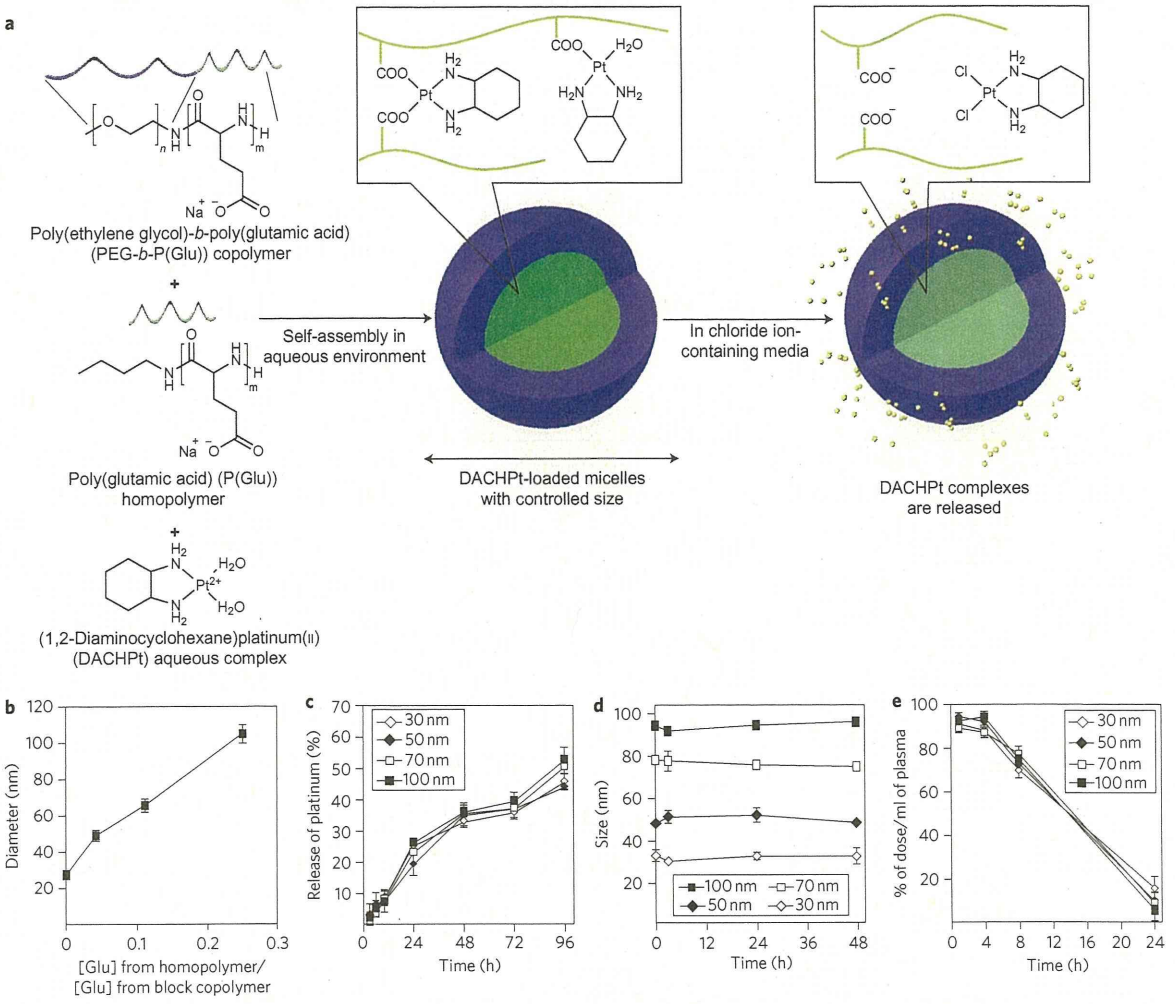

Figure 1 | Construction and physicochemical properties of DACHPt-loaded micellar nanomedicines (DACHPt/m) with different diameters. a, Schematic showing DACHPt/m formed through the interaction between DACHPt and the carboxylic groups of poly(glutamic acid) (green) in PEG-*b*-P(Glu) and P(Glu). In media containing chloride ions, DACHPt (yellow circles) is released from the micelles through ligand exchange between the carboxylic groups in P(Glu) and the chloride ions. **b**, Changing micelle size by altering the ratio of P(Glu) from the homopolymer and the P(Glu) portion of PEG-*b*-P(Glu) in the mixture. Total glutamic acid residue concentration was maintained at 5 mM. **c**, Micelles of all sizes release DACHPt at similar rates. **d**, Micelles of all sizes incubated in cell culture media containing 10% serum at 37 °C maintained their sizes over 48 h. **e**, Plasma clearances of micelles with different diameters follow similar trends. Data are means ± s.e.m., $n = 3$.

Table 1 | Diameter, size distribution, drug loading and surface charge of 30, 50, 70 and 100 nm micelles.

Size (nm)*	Polydispersity index	[Pt]/[COO] (mol/mol)†	Pt/polymer (wt/wt%)	Zeta-potential (mV)‡
30	0.16	0.56	34	−2.29 ± 1.41
54	0.14	0.6	48	−1.61 ± 0.58
69	0.12	0.57	54	−0.89 ± 0.33
110	0.11	0.52	69	0.15 ± 0.21

*Determined by DLS. †Determined by ICP-MS (platinum concentration) and weight of micelles. ‡Determined by laser doppler electrophoresis ($n = 4$, mean ± s.d.).

The 30, 50, 70 and 100 nm DACHPt/m presented similar zeta potentials, ranging from −2.29 to 0.15 mV at pH 7.4 (Table 1). These micelles showed similar drug release rates (Fig. 1c), driven by the ligand exchange of DACHPt between the carboxylic groups of P(Glu) and the chloride ions in the biological media. After 96 h incubation in cell culture media containing 10% fetal bovine serum (FBS) at 37 °C, the drug release from DACHPt/m reached ~50% (Fig. 1c). Under similar conditions, differently sized DACHPt/m maintained their diameters for over 48 h (Fig. 1d). DACHPt/m of different sizes also showed similar plasma clearance rates (~12% of injected dose (ID) per ml plasma remained after 24 h) and plasma half-lives (7–8 h) (Fig. 1e and Supplementary Table S1, respectively). We recently showed that DACHPt/m can maintain their micellar structure in the circulation for at least 24 h after injection[28]. Furthermore, DACHPt/m of varying sizes show similar distributions in the kidney, liver and spleen (Supplementary Fig. S2 and

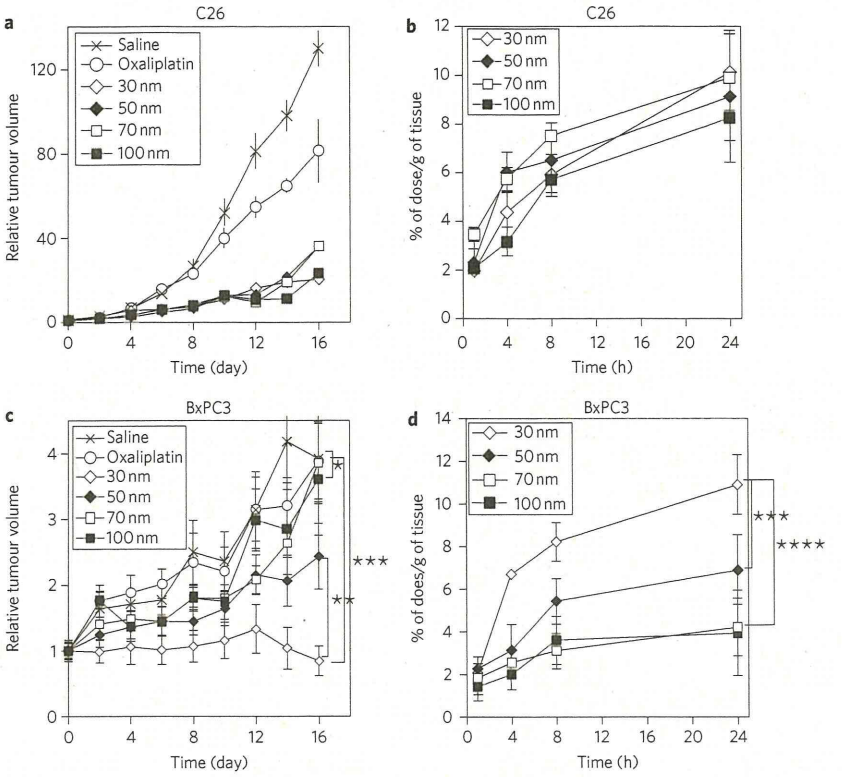

Figure 2 | Anticancer activity and tumour accumulation of DACHPt/m with different diameters. a–d, Plots of relative tumour volumes of subcutaneous hyperpermeable murine colon adenocarcinoma (C26) (**a**) and subcutaneous hypopermeable human pancreatic adenocarcinoma BxPC3 (**c**) tumours, and accumulation of DACHPt/m in C26 (**b**) and BxPC3 (**d**) tumours. To evaluate antitumour activity, oxaliplatin was injected on days 0, 2 and 4 (dose, 8 mg kg^{-1}) and micelles were injected on days 0, 2 and 4 (dose, 3 mg kg^{-1} on a platinum basis). For tumour accumulation experiments, micelles were injected at 100 μg per mouse on a platinum basis. Data are means ± s.e.m., $n = 6$. *$P > 0.05$; **$P < 0.05$; ***$P < 0.01$; ****$P < 0.001$.

Table S1), which are the major organs responsible for the clearance of nanocarriers[29]. The levels of accumulation of DACHPt/m in these organs are comparable to other polymeric micelles incorporating cisplatin[8] or doxorubicin[9], except for a slightly higher accumulation of 100 nm DACHPt/m in the liver. Because the surface chemistry and charge of nanocarriers have been reported to critically affect the interactions of nanocarriers with plasma proteins and cells and the biodistributions of nanocarriers[21,22,29,30], the analogous surface chemistry (PEG-coated surface), neutral charge and comparable plasma clearance of DACHPt/m with different diameters are substantial advantages for the evaluation of their extravasation, penetration and accumulation abilities in solid tumours as well as the associated therapeutic outcomes.

Antitumour activity of DACHPt/m in solid tumours

The antitumour activity and accumulation of DACHPt/m with different diameters were examined in tumour models with different permeabilities: a hyperpermeable murine colon adenocarcinoma 26 (C26) model characterized by high vascularization and slight tumour stroma[31] and a human pancreatic adenocarcinoma BxPC3 characterized by low vascularization, reduced vascular permeability due to pericyte coverage of blood vessels[20,31] and thick fibrosis, which are representative characteristics of some intractable solid tumours[20,31–33]. Note that the *in vitro* cytotoxicity of sub-100 nm DACHPt/m on C26 and BxPC3 cell lines was not substantially affected by micelle size (Supplementary Table S3), suggesting that their *in vivo* antitumour effect can be associated with their accumulation and microdistribution in solid tumours. In the C26 model, all micelles demonstrated comparable tumour growth inhibition (Fig. 2a), whereas oxaliplatin did not show a significant antitumour effect. The accumulation levels of all sub-100 nm micelles in C26 tumours were consistently comparable, reaching ~10% ID g^{-1} tumour at 24 h post-injection (Fig. 2b). In the BxPC3 model, the size effect of DACHPt/m on antitumour activity became evident, with the 30 nm micelles completely suppressing tumour growth, the 50 nm micelles leading to reduced antitumour activity, and the 70 nm and 100 nm micelles failing to show any antitumour effect (Fig. 2c). The accumulation of the 30 nm micelles was two times higher than that of the 50 nm micelles and four times higher than that of the 70 and 100 nm micelles after 24 h in BxPC3 tumours (Fig. 2d), which is also consistent with the antitumour efficacies in Fig. 2c.

The intratumoral microdistribution of fluorescently labelled DACHPt/m with different sizes in tumour sections was studied to investigate size-dependent extravasation and penetration of micellar nanomedicines in tumours. Histological investigations using haematoxylyn and eosin (H&E) staining revealed a well-vascularized medullary histological pattern of C26 tumours with reduced tumour stroma (Fig. 3a). In this tumour model, the fluorescence signals from the 30, 50, 70 and 100 nm micelles were uniformly distributed throughout the entire section at 24 h post-injection, suggesting deep tumour penetration of all sub-100 nm micelles (Fig. 3b, red). The immunofluorescence localization of platelet endothelial cell adhesion molecule-1 (PECAM-1), expressed by endothelial cells, indicated the extensive distribution of blood vessels in C26 tumours (Fig. 3b, green). However, H&E staining of BxPC3 tumours revealed the formation of nests of cancer cells surrounded by fibrotic tissue (Fig. 3c), which may act as a barrier